

# DMSO hydration redefined: unravelling the hydrophobic hydration of solutes with a mixed hydrophilic–hydrophobic characteristic

A. Panuszko, P. Bruździak, M. Śmiechowski, M. Stasiulewicz, J. Stefaniak,  
and J. Stangret\*

*Department of Physical Chemistry, Gdańsk University of Technology, Narutowicza  
11-12, 80-233 Gdańsk, Poland*

---

## Abstract

Hydrophobic hydration of solutes with a mixed hydrophilic–hydrophobic characteristics is still poorly understood. This is because both experimental and theoretical methods find it difficult to see the ice-like water structure around the nonpolar solute groups, unlike hydrogen bonds with the hydrophilic groups. In order to unravel this problem, we have investigated DMSO hydration by means of infrared spectroscopy and theoretical methods, namely DFT, ONIOM calculations and AIMD simulations, which allowed us to redefine its hydration. In dilute DMSO solutions the clathrate-like water is formed around the DMSO molecule, supported by interactions of water molecules with the methyl hydrogens (the blue-shifted hydrogen bonds). The cage is constructed by water molecules that form hydrogen bonds of the comparable energy and length with the SO group and between water molecules. When the construction of the cage is completed, DMSO molecule partially regains its rotational freedom inside. Strong hydrogen bonds within the frame

---

\*janusz.stangret@pg.edu.pl

are masked by the relatively small population of weakened hydrogen bonds of water molecules in the vicinity of the SO group, due to the improper fit to the bulk water of water molecules hydrogen bonded to the oxygen atom of DMSO. We also propose a new explanation of the highly non-ideal mixing behavior of aqueous DMSO solutions at the eutectic point, as the positive excess entropy of the equimolar amounts of molecular complexes distinguished in the system.

*Keywords:* Water structure, Hydrophobic hydration, DMSO-water complexes, FTIR spectroscopy, DFT calculations, AIMD simulations

---

## **1. Introduction**

“Water is an active matrix of life for cell and molecular biology” [1]. In this sense, the role of water relies on its diverse structural and dynamic characteristics in such systems. One of the very important specific structural forms which water adopts near non-polar surfaces of biomolecules is known as the hydrophobic hydration which contributes to many chemical and biochemical processes, such as protein folding, protein–protein, and protein–co-solute or self-assembly of lipid membranes [2, 3, 4, 5, 6, 7, 8, 9, 10]. However, since the formulation of the “iceberg formation” hypothesis by Frank and Evans [11], opinions on the water structure near the non-polar fragments of solutes have been inconsistent (see for example ref. [12] for a review). Recently, their model has been confirmed by Grdadolnik *et al.* [13] by means of the high-pressure infrared spectroscopy for small purely hydrophobic solutes (methane, ethane, krypton, and xenon). The strengthened water structure in such cases is similar to the one of ice or solid clathrates. Other direct

16 experimental evidence has also been demonstrated [14, 15], however, studies  
17 of soluble solutes with both hydrophilic and hydrophobic moieties elude any  
18 simple explanation of their complex hydration [16, 17]. Dimethyl sulfoxide  
19 (DMSO) is a simple molecule which can serve as a model for studying such  
20 a type of mixed hydration.

21 DMSO is an aprotic solvent and its aqueous solutions have many inter-  
22 esting physicochemical and biological properties. DMSO is miscible with  
23 water in all proportions [18]. Dielectric spectroscopy studies of liquid DMSO  
24 have proven the existence of its dimers and longer forms (“polymers”) with  
25 anti-parallel ordering of molecular dipoles [19, 20]. Numerous studies have re-  
26 vealed uncommon physicochemical properties of DMSO–water system, man-  
27 ifested by strong deviations of their thermodynamic properties from ide-  
28 ality [21]. Many reports indicate that water–DMSO hydrogen bonds are  
29 stronger than those between water molecules [19, 20, 22]. As a result of  
30 these interactions, molecular complexes of water and DMSO are relatively  
31 stable, regardless of composition [23]. It is assumed that the unusual features  
32 of DMSO solutions are due to the various species water–DMSO complexes  
33 [24, 25]. These clusters at various DMSO concentrations have been exten-  
34 sively studied both experimentally [20, 21, 26, 24, 25, 27] and theoretically  
35 [23, 24, 28, 29, 30, 31]. Those which consist of  $3\text{DMSO}\cdot1\text{H}_2\text{O}$ ,  $2\text{DMSO}\cdot1\text{H}_2\text{O}$ ,  
36 and  $1\text{DMSO}\cdot1\text{H}_2\text{O}$  have been found at mole fractions of water ( $x_w$ ) lower than  
37 0.5 [21, 23, 25]. The strongest deviations from ideality and the strongest hy-  
38 drogen bonds occur at  $x_w$  between 0.6 and 0.7 [26, 32, 17]. The presence  
39 of stable  $1\text{DMSO}\cdot2\text{H}_2\text{O}$  aggregate has been observed in this range [20, 26].  
40 It is also the eutectic composition with freezing temperature of ca.  $-70^\circ\text{C}$

<sup>41</sup> [33], while freezing points of water and DMSO are 0 °C and 18.6 °C, respec-  
<sup>42</sup> tively. But according to the hypothesis of Kirchner and Reiher [31], many  
<sup>43</sup> energetically similar but structurally different complexes exist in the DMSO–  
<sup>44</sup> water mixture near the eutectic point. They proposed the mechanism of the  
<sup>45</sup> clusters' influence on the non–ideal mixing behavior of these systems.

<sup>46</sup> There is no general agreement on the influence of DMSO on water struc-  
<sup>47</sup> ture. The results of experimental studies [34, 35, 36, 37] and computer sim-  
<sup>48</sup> ulations [28, 35, 38, 39] indicate that water structure is enhanced in dilute  
<sup>49</sup> DMSO aqueous solutions. On the other hand, some experimental studies  
<sup>50</sup> [20, 40, 41] lead to the conclusion that water structure is weakened at a low  
<sup>51</sup> concentration of DMSO. The experimental techniques, including IR spec-  
<sup>52</sup> troscopy and MD simulations demonstrate that DMSO acts as a “structure  
<sup>53</sup> breaker” at high concentrations of DMSO [28, 37].

<sup>54</sup> In this paper, we examine the hydration of dimethyl sulfoxide (DMSO)  
<sup>55</sup> in the whole mole fraction range by means of the FT-IR spectroscopy and  
<sup>56</sup> computational methods. We demonstrate the existence of the “ice-like” water  
<sup>57</sup> cage around DMSO molecules in diluted solutions, which enables partial  
<sup>58</sup> rotational freedom of the guest molecule inside the water cage. We propose  
<sup>59</sup> also a novel explanation of the strong deviation from ideality of aqueous  
<sup>60</sup> solutions of DMSO at concentration corresponding to the eutectic point of  
<sup>61</sup> the system.

62 **2. Materials and methods**

63 *2.1. Chemicals and solutions*

64 Dimethyl sulfoxide (99.9%, Alfa Aesar) and D<sub>2</sub>O (isotopic purity 99.9%,  
65 Aldrich) were used as supplied to prepare solutions without purification.  
66 Water used to prepare these solution was deionized (<0.01 S·cm<sup>-1</sup>). All  
67 solution have been prepared by weight and their densities were determined  
68 with Anton Paar DMA 5000 densitometer at 25.000 ± 0.001 °C. The solution  
69 preparation procedure for FTIR measurements of HDO spectra has been  
70 described in Supporting Material in ref. [42].

71 *2.2. FTIR spectroscopy*

72 All FTIR spectra of aqueous solutions of DMSO were recorded on the  
73 IFS 66 Bruker spectrometer. The spectrometer was purged with dry nitro-  
74 gen during the measurement. A liquid transmission cell (model A145, Bruker  
75 Optics) was equipped with two CaF<sub>2</sub> windows separated by teflon spacers.  
76 For H<sub>2</sub>O transmission spectra of DMSO-water mixtures for high concentra-  
77 tion of DMSO (in the range of ν<sub>S=O</sub> vibration), 512 independent scans were  
78 taken with resolution of 2 cm<sup>-1</sup>. The path length was equal to 0.0053 mm, as  
79 determined interferometrically. In the case of HDO spectra, in the range of  
80 ν<sub>OD</sub> vibration 256 independent scans were taken with the resolution of 4 cm<sup>-1</sup>.  
81 The path length was equal to 0.0306 mm, as determined interferometrically.  
82 The same path length was used also in the case of spectra for DMSO·H<sub>2</sub>O  
83 mixtures for very low DMSO concentration, in the range of the ν<sub>S=O</sub> vibra-  
84 tion band. The temperature was kept at 25.0 ± 0.1 °C and monitored using  
85 thermocouples placed in the sample cell.

86        The spectra have been analyzed using the following commercial software:  
87        GRAMS/32 (Galactic Industries Corp.) and RAZOR (Spectrum Square As-  
88        sociates, Inc.) run under GRAMS/32.

89        *2.3. Analysis of vibrational spectra*

90        The difference spectra method was applied to extract the DMSO-affected  
91        HDO spectrum on the basis of spectra series measured for different molalities  
92        of aqueous solutions. An assumption was made that the water in solution can  
93        be divided into two additive contributions: the bulk water (pure water) and  
94        the “solute-affected” water (modified by interactions with the solute). The  
95        method of analysis of the spectral data towards extraction of solute-affected  
96        water spectrum was described in details in refs. [43, 44, 45] and some of  
97        the most basic information are included in the Supplementary Material. The  
98        difference spectra method was also applied to the DMSO spectra in the range  
99        of the  $\nu(\text{S=O})$  vibrations to separate specific states of the S=O oscillators.

100       The factor analysis, in the version written by Malinowski [46], was per-  
101       formed using the commercial computer program Factor Analysis Toolbox for  
102       MATLAB (Applied Chemometrics Inc., Sharon). The spectral data were  
103       assembled into matrices of absorbances at given wavenumbers and concen-  
104       trations of DMSO–water mixtures. The main application of this method  
105       was window factor analysis (WFA) [47], which involves the extraction of the  
106       concentration profiles of the individual chemical species contributing to the  
107       spectral data (i.e. factors). The correct number of these factors was obtained  
108       by using the basic principal factor analysis algorithm (PFA).

109 2.4. Theoretical calculations

110 2.4.1. DFT and ONIOM calculations

111 All calculations were performed with the GAUSSIAN 09 v.D1 software  
112 [48] available at the Academic Computer Center in Gdansk (TASK). The  
113 program Avogadro was used to prepare of input data and for visualization  
114 of computed results. The analysis of resulting wavefunction files, involving  
115 the reduced density gradient (RDG) method [49], was performed with the  
116 Multiwfn software v.3.3.9 [50]. The RDG method allowed to visualize weak  
117 interaction sites (hydrogen bonds, van der Waals interactions, steric clashes)  
118 in molecular complexes and to classify them according to their strengths.  
119 All RDG-related figures are presented in the stereo view for better clarity.  
120 The D3 version of Grimme's empirical dispersion correction, including the  
121 Becke–Johnson damping (GD3-BJ), was applied [51].

122 Structures of medium-sized complexes: 1DMSO·nH<sub>2</sub>O (where n = 1÷15),  
123 3DMSO·2H<sub>2</sub>O, and 3DMSO were optimized using the density functional  
124 theory (DFT) level with the B3LYP hybrid exchange-correlation functional  
125 [52, 53] and 6-311++G(d,p) basis set [54]. The conductor-like polarizable  
126 continuum model (CPCM) of the self-consistent reaction field theory (SCRF)  
127 was used to simulate the solvent environment [55, 56]. In the case of three  
128 different types of the considered complexes: 1DMSO·nH<sub>2</sub>O, 3DMSO·2H<sub>2</sub>O,  
129 and 3DMSO, the following solvents were used: water, solvent mixture of  
130 DMSO:water with a mixing ratio of 3:2, and DMSO, respectively.

131 For more complex structures of one DMSO molecule with up to 100 hy-  
132 dration water molecules the ONIOM approach was applied [57]. 5 to 90 water  
133 molecules were added to the DMSO molecule with a step of 5 molecules. Ad-

<sup>134</sup> ditional complexes with 2 to 4 molecules were prepared, however, a more re-  
<sup>135</sup> liable results for such complexes were obtained with the method presented in  
<sup>136</sup> previous paragraph thanks to the larger basis set and the use of the CPCM  
<sup>137</sup> solvent model. Initial complexes were optimized with a simple MMFF94a  
<sup>138</sup> force field [58, 59]. Next, the central DMSO molecule was selected for the high  
<sup>139</sup> level of ONIOM calculations – B3LYP/aug-cc-pVQZ, and all water molecules  
<sup>140</sup> for the low level – B3LYP/cc-pVDZ, all performed *in vacuo*. Such a selec-  
<sup>141</sup> tion of basis sets allowed to obtain satisfactory structures within a reasonable  
<sup>142</sup> calculation time.

<sup>143</sup> Three different water clusters have been used to obtain the reference  
<sup>144</sup> parameters for hydrogen bonds energies between solvent molecules: 1) a  
<sup>145</sup> triangle prism, or nano-drop of 6 molecules for medium-sized complexes, 2)  
<sup>146</sup> an unstructured complex of 100 molecules for ONIOM-based calculations.

#### <sup>147</sup> 2.4.2. AIMD simulations

<sup>148</sup> AIMD simulations [60] were performed using the DFT-based QUICKSTEP  
<sup>149</sup> electronic structure module [61] of the CP2K 6.0 computational suite [62,  
<sup>150</sup> 63]. We applied the BLYP functional [52, 64] together with the DFT-D3  
<sup>151</sup> empirical dispersion correction [65]. The cutoff for the latter was set to 16 Å.  
<sup>152</sup> QUICKSTEP defines a mixed Gaussian type orbitals plus plane waves (GPW)  
<sup>153</sup> basis set scheme [66], and we used a TZV2P basis set for atomic orbitals  
<sup>154</sup> and a 500 Ry cutoff for the plane wave expansion of the electron density.  
<sup>155</sup> Only valence electrons were treated explicitly, while the core electrons were  
<sup>156</sup> represented by GTH pseudo potentials [67].

<sup>157</sup> The two studied systems consisted of bulk H<sub>2</sub>O (80 molecules) and a  
<sup>158</sup> DMSO(H<sub>2</sub>O)<sub>80</sub> solution, contained in cubic supercells with applied periodic

boundary conditions. In order to compare directly to the FTIR HDO/H<sub>2</sub>O spectra, all water hydrogen atoms were given the mass of deuterium, i.e., we effectively simulate D<sub>2</sub>O. Initial volumes of the systems were chosen to reflect the experimental density of heavy water [68] combined the apparent molar volume of the DMSO solution [69]. While the experimental data were measured at 298 K, we apply a slight temperature overscaling, typical for AIMD simulations neglecting nuclear quantum effects, in order to recover the proper diffusional behavior of individual molecules in our systems and to avoid the ‘glassy dynamics’ regime [70]. The extent of this scaling is slight for D<sub>2</sub>O ( $T = 323.15$  K)[71].

Both systems were first equilibrated for at least 20 ps with a time step of 0.5 fs in the *NVT* ensemble using massive Nosé-Hoover chain thermostatting [72]. After the equilibration period, 20 initial conditions were sampled every 3 ps from a further *NVT* simulation to initialize microcanonical (*NVE*) trajectories of 20 ps length each. During these runs the centers of maximally localized Wannier functions (MLWFs) [73] were computed every 2 fs. All analyzed observables were averaged over the *NVE* trajectories yielding proper canonical averages.

Molecular dipole moments were obtained classically by summing over positive nuclei and negative MLWF centers. The IR spectra were calculated as Fourier transforms of time correlation functions of dipole moment finite differences [74, 75] using various recently introduced dipolar decomposition schemes for solute–solvent systems, see refs. [75, 76] for details. The spectral resolution was set to 1 cm<sup>-1</sup> by setting the upper limit of the correlation time to  $\sim 16.66$  ps and the final spectra were smoothed by passing through

<sup>184</sup> a  $20\text{ cm}^{-1}$  Gaussian filter. Numerical Kramers–Krönig transform was used  
<sup>185</sup> to remove the refractive index contributions to the IR spectra [75] using the  
<sup>186</sup> experimental refractive index of  $\text{D}_2\text{O}$ ,  $n_{\text{D}} = 1.328$  [77].

<sup>187</sup> **3. Results and discussion**

<sup>188</sup> *3.1. FTIR spectra of HDO in DMSO-water mixtures*

<sup>189</sup> HDO spectra in the range of the  $\nu(\text{OD})$  vibrations are shown for all com-  
<sup>190</sup> positions of the DMSO–water mixture in Fig. 1a. It is clear that the spectral  
<sup>191</sup> series exhibits two isosbestic points: the first one at ca.  $2600\text{ cm}^{-1}$  corre-  
<sup>192</sup> sponding to the spectra from pure water to  $x_w = 0.83 \pm 0.07$ , and the second  
<sup>193</sup> one at ca.  $2530\text{ cm}^{-1}$  corresponding to spectra from the smallest dilutions of  
<sup>194</sup> water in DMSO to  $x_w = 0.41 \pm 0.01$ .

<sup>195</sup> The main parameters of the HDO spectra as a function of  $x_w$  are presented  
<sup>196</sup> in Fig. 1b (and also in the Supplementary Material, see Fig. S2). Particularly  
<sup>197</sup> noteworthy is the dependence for  $\nu(\text{OD})$  band position at maximum and at  
<sup>198</sup> the center of gravity of the band. The first one serves as a measure of  
<sup>199</sup> the most probable energy of hydrogen bonds of water (as well as the most  
<sup>200</sup> probable  $\text{O}\cdots\text{O}$  distance), and the latter as a measure of the average energy  
<sup>201</sup> of hydrogen bonds (as well as the average  $\text{O}\cdots\text{O}$  distance).

<sup>202</sup> —Figure 1—

<sup>203</sup> In simple terms, DMSO dissolved in water in larger quantities should be  
<sup>204</sup> classified as a water “structure-breaking” solute. Only in the range of high  
<sup>205</sup> dilutions, above ca. 0.8 mole fraction of water, DMSO can be considered  
<sup>206</sup> as a “structure-making” agent. This may be inferred from the position of  
<sup>207</sup> the center of gravity of the  $\nu(\text{OD})$  band, which is red-shifted relative to the

pure water, Fig. 1b. This conclusion is in agreement with other IR studies [37]. The DMSO–water interaction is stronger than water–water interaction: the energy of vaporization of water from DMSO (infinitely diluted solution of water) equals to  $46.87 \text{ kJ}\cdot\text{mol}^{-1}$  vs.  $41.53 \text{ kJ}\cdot\text{mol}^{-1}$ , which corresponds to the energy of vaporization of pure water [78]. The results of the DFT calculations confirm this result: interactions of water molecules with the oxygen atom of S=O group are stronger than those between water molecules in the pure water (see Fig. S7 in the Supplementary Material). This is also in agreement with the structural data obtained from the AIMD simulations: the O···O distance in pure D<sub>2</sub>O is 0.02 Å longer than the O<sub>DMSO</sub>···O<sub>D<sub>2</sub>O</sub> distance; see Fig. S10 and Table S2 in the Supplementary Material. On the other hand, this is a typical situation for the aprotic solvent–water systems for which solvent–water interactions are stronger than water–water interactions [78, 79]. Further explanation can be found in the Supplementary Material (section S1.3).

### 3.1.1. DMSO-affected HDO spectra at high water concentration

Fig. 2a shows DMSO-affected HDO spectra for high water content in the mixtures, along with the affected spectrum obtained for solution of DMSO infinitely diluted in water, the bulk HDO and the dependence of the affected number (i.e. number of moles of water molecules affected by one mole of DMSO,  $N$ ), on the water mole fraction (see the inset). It should be noted that this parameter generally does not correspond to a hydration number in strict sense, it rather shows the number of solvent molecules statistically influenced by a solute. Because of lability of the hydration sphere for the most of solutes, only a few water molecules appear to be influenced in their proximity, the rest

resembling bulk water. This way, the solute-affected spectrum represents the water status in the “concentrated form”. As it can be seen in Fig. 2a, DMSO-affected  $\nu(\text{OD})$  band positions are blue-shifted relative to the bulk water and, on visual inspection, do not show complex structure. The most interesting seems to be the variability of the derivatives  $(d\varepsilon(\nu)/dm)_{m=m_i}$  obtained for the molalities of DMSO ( $m_i$ ) corresponding to the water mole fractions shown in the inset in Fig. 2a. The derivative corresponding to the infinite dilution of DMSO in water ( $m_i = 0$ ) is characterized by two occurrences of the maximum increase of absorption: (1) at  $2538 \text{ cm}^{-1}$ , which belongs to water molecules with weaker hydrogen bonds than in the bulk water, and (2) at  $2438 \text{ cm}^{-1}$ , which corresponds to the strong hydrogen bands of water, as in the case of ice [13]. The last component quickly loses its intensity with the increase of DMSO content in solution and virtually disappears at  $x_w \simeq 0.85$ , while the first component remains at its place.

—Figure 2—

For further discussion of the observed spectral effects, we will use the transformation of the DMSO-affected water band-shape to the interatomic oxygen–oxygen ( $\text{O}\cdots\text{O}$ ) distance distribution function between water molecules,  $P(R_{OO})$ , as described in ref. [45]. The “O” symbol can also denote the oxygen atom of the  $\text{S}=\text{O}$  group, when the oxygen atom of this group is hydrogen bonded with water molecules. Fig. 2b shows the differences in interatomic  $\text{O}\cdots\text{O}$  distance distribution functions,  $\Delta P(R_{OO})$ , between DMSO-affected water (for water at infinite dilution or for water at  $x_w \simeq 0.85$ ) and the bulk water. These differences qualitatively resemble the features of the evolution of the derivative  $(d\varepsilon(\nu)/dm)_{m=m_i}$  in Fig. 2a. However, the difference deter-

258 mined for DMSO-affected water at  $x_w \simeq 0.85$ ,  $\Delta P(R_{OO})_{x=0.85}$  (Fig. 2b), still  
259 shows an increase of the population of water at short O···O distances, corre-  
260 sponding to the ice-like structure, but this population is much smaller than  
261 for the solution at infinite dilution.

262 As the water concentration increases ( $x_w > 0.85$ ), the water cage around  
263 DMSO molecule develops, thus increasing the population of strong hydrogen  
264 bonds between the water molecules surrounding the methyl groups. This  
265 increase is illustrated by the derivative  $(d\varepsilon(\nu)/dm)_{m=m_i}$  (Fig. 2a) and the  
266  $\Delta\Delta P(R_{OO})$  function (Fig. 2b). The structural and energetic state of the  
267 DMSO hydration water at the infinitely diluted solution is characterized by  
268 the  $\Delta P(R_{OO})_{x=1}$  function in Fig. 2b. Accordingly, it should be assumed that  
269 for  $x_w > 0.85$  strong hydrogen bonds are formed by water molecules both  
270 (1) interacting with the S=O group of DMSO, as well as (2) participating  
271 in the hydrogen bond network around methyl groups. These two groups  
272 of strongly bound water molecules were confirmed by DFT calculation (see  
273 Fig.S7 in Supplementary Material). As it can be seen, in terms of the O···O  
274 distance both types of hydrogen bonds are poorly distinguishable for small  
275 hydration complexes. However, a tendency can also be observed for hydrogen  
276 bonds with the S=O group to become weaker as the water cage develops.  
277 Only a small population of the water molecules in the hydration shell can  
278 be regarded as weakened, as evidenced by the presence of a maximum at  
279 ca. 2.90 Å in the  $\Delta P(R_{OO})_{x=1}$  function. This population is also visible on  
280 the corresponding difference obtained from AIMD simulation (Fig. 3b) and  
281 reflects the water–water hydrogen bonds around the DMSO oxygen atom  
282 (explanation in section 3.1.2).

283     3.1.2. Confrontation of experimental results with those obtained from AIMD  
284       simulations

285     It is most instructive to confront the experimental HDO spectra in the  
286     ν(OD) range with the computational IR spectra of D<sub>2</sub>O obtained from AIMD  
287     simulations (see section S4.4 in the Supplementary Material for implementa-  
288     tion details). The representative distance-dependent IR spectra that selec-  
289     tively capture the absorption of the solute–water complex up to a specified  
290     cutoff radius  $R_c$  are shown in Fig. 3a. Simultaneously, the hydrogen bond  
291     definitions (see section S4.1 in the Supplementary Material) have been used  
292     to obtain interatomic oxygen–oxygen distance distribution functions corre-  
293     sponding to the experimental ones.

294     —Figure 3—

295     Compared to the experimental liquid D<sub>2</sub>O spectrum [80], the respective  
296     IR spectrum computed on the basis of AIMD simulations is red-shifted by  
297     ~ 90 cm<sup>-1</sup>. This magnitude of the red shift is typical of the liquid wa-  
298     ter simulations using the generalized gradient approximation (GGA)-based  
299     functionals [76, 81] and in explicit inclusion of nuclear quantum effects (NQE)  
300     is required to obtain a better agreement with experiment [82, 83]. However,  
301     even in the absence of NQE the band shifts obtained from the distance-  
302     dependent spectra can be meaningfully compared to experiment [76, 84].

303     We first focus on the spectrum of DMSO molecule extracted from the  
304     aqueous solution. As demonstrated previously, such spectra record important  
305     information about the hydration shell due to the dipole moment induced  
306     by the solvent’s local electric field and the appearance of the thus allowed  
307     vibrational transitions in the IR spectrum [76, 84]. In the case of DMSO,

308 the band position at maximum is blue-shifted by  $44\text{ cm}^{-1}$ . Coincidentally,  
309 this is in perfect agreement with the experimental  $\nu(\text{OD})$  band shift for HDO  
310 infinitely diluted in DMSO (section S1.3 in Supplementary Material). Since  
311 for other hitherto studied solutes similar effects can be observed (i.e., the  
312 band shift in the distance-dependent IR spectra is the most pronounced at  
313 the vanishing cutoff radius), we hypothesize now that the solute molecule  
314 extracted from the solution encodes in a unique way the energetic state of  
315 the water molecules at their most perturbed state in the solution, such as at  
316 the limit of the infinite dilution in the given solvent.

317 With the increasing cutoff radius, the distance-dependent IR spectra un-  
318 dergo major changes in the position and the intensity of the water stretching  
319 band [76]. These changes can be monitored selectively at a chosen probe  
320 wave number, here taken as the position at maximum of the band at  $R_c \rightarrow 0$ ,  
321  $\nu^\circ = 2461\text{ cm}^{-1}$ ; see inset in Fig. 3a. With increasing  $R_c$ , the intensity of  
322 the  $\nu(\text{OD})$  band also increases and reaches a local maximum at  $R_c = 3.8\text{ \AA}$ .  
323 This particular cutoff radius is then selected as the most representative of  
324 the DMSO–water complex. The  $\nu(\text{OD})$  band position at maximum at this  
325  $R_c$  is blue-shifted by  $16\text{ cm}^{-1}$ , in excellent agreement with the experimentally  
326 observed shift by  $11\text{ cm}^{-1}$  ( $2519\text{ cm}^{-1}(\nu^\circ_{\text{DMSO}}) - 2508\text{ cm}^{-1}(\nu^\circ_{\text{bulk}})$ , values for the  
327 infinite dilution solution, see Table S1 in Supplementary Material). Simulta-  
328 neously, we can obtain the normalization factor for the distance-dependent  
329 IR spectra and thus determine the fractional number of water molecules in  
330 the considered solute-centered sphere. It is found to be equal to  $3.2 \pm 0.6$   
331 (the uncertainty is based on the uncertainty of the  $R_c$  value,  $\pm 0.1\text{ \AA}$ ), also  
332 in perfect correspondence with the experimental affected number  $N = 2.8$

333 (value for the infinite dilution solution, see inset in Fig. 2a and Table S1 in  
334 Supplementary Material). Thus, our distance-dependent IR spectra firmly  
335 support the results of the analysis of the experimental data with the affected  
336 spectra method.

337 To further explore the parallel character of experimental and computa-  
338 tional IR spectra, we again turn to the interatomic oxygen–oxygen ( $\text{O}\cdots\text{O}$ )  
339 distance distributions; see Fig. 3b. We monitor the changes in the geom-  
340 etry of the hydrogen bond network with respect to bulk water by applying  
341 the distance distribution differences,  $\Delta P(R_{OO})$ , by analogy to the analysis  
342 of experimental spectra (section 3.1.1). By selectively computing  $P(R_{OO})$   
343 functions around specific sites of DMSO, the local state of the hydrogen  
344 bond network can be revealed. As seen in Fig. 3b, the distance distributions  
345 around DMSO oxygen undergo much more pronounced changes than around  
346 the methyl groups. Interestingly, the  $\text{O}_{\text{DMSO}}\cdots\text{O}_{\text{water}}$  hydrogen bonds show  
347 a completely different trend that the water–water hydrogen bonds in which  
348 water molecules located in the first hydration shell around DMSO oxygen  
349 are involved. While the former are found to be strengthened with respect  
350 to the bulk water, in accordance with the previously discussed DFT studies  
351 of static aqueous clusters (see Fig. S7 in the Supplementary Material), the  
352 latter are weakened, possibly because the water molecules involved in short  
353 hydrogen bonds with  $\text{O}_{\text{DMSO}}$  have trouble with incorporating into the ex-  
354 tended hydrogen bond network. The weakening of hydrogen bonds of water  
355 is also illustrated in the appropriate distance distribution difference obtained  
356 from the spectral data Fig. 2b. On the other hand, the water–water hydrogen  
357 bonds around the hydrophobic groups show only a slight reduction of weak

358 elongated hydrogen bonds with the corresponding appearance of medium-  
359 and short-length bonds, but this behavior is qualitatively in agreement with  
360 the discussion of the experimental results presented above. We note that  
361 similar enhancement of the hydrogen bond network around the hydrophobic  
362 groups of TMAO has been recently found [85].

363 *3.2. FTIR spectra of DMSO in aqueous solutions*

364 *3.2.1. Spectra in the range of  $\nu(S=O)$  vibrations*

365 The results of FTIR studies of DMSO–water mixtures in the entire com-  
366 position range for the  $\nu(S=O)$  band are summarized in Fig. 5. Spectra shown  
367 in Fig. 5a correspond to the  $\nu(S=O)$  vibrations in the 975–1150  $\text{cm}^{-1}$  range,  
368 while the band at ca. 950  $\text{cm}^{-1}$  is due to the rocking vibrations of DMSO  
369 methyl groups [86]. The assignment of the two low-wavenumber components  
370 of the complex band of the  $\nu(S=O)$  vibrations solely to the methyl rocking  
371 modes, as in refs [25, 87, 88], is not justified in view of the most recent reas-  
372 signment which concludes that the  $\text{CH}_3$  rocking modes are actually tightly  
373 coupled with the  $\nu(S=O)$  band [89].

374 —Figure 5—

375 As it can be seen in Fig. 5a, the addition of water to DMSO signifi-  
376 cantly changes the shape and the position of the  $\nu(S=O)$  band. Generally,  
377 the increase of water mole fraction ( $x_w$ ) results in the decrease of the high-  
378 wavenumber component of the SO band (band fitting procedure indicates  
379 that this component disappears at  $x_w \simeq 0.6$ ), while the other two compo-  
380 nents are red-shifted and their total intensity increases. It is difficult to  
381 identify their individual behavior, because most probably these component  
382 bands exchange positions at  $x_w \simeq 0.4$ . The overall spectral changes observed

383 in the case of these two component bands are typical for the proton accep-  
384 tor group forming a hydrogen bond, in this case with water molecules. Our  
385 AIMD simulations show that (at  $x_w \simeq 0.988$ ) on average 2.5 hydrogen bonds  
386 are formed between the DMSO oxygen and the water molecules; see Figs. S8  
387 and S9 in the Supplementary Material. It is worth noting that the band at  
388 ca.  $950\text{ cm}^{-1}$  exhibits a similar behavior. When the mole fraction of water  
389 exceeds ca. 0.98 (water to DMSO molar ratio higher than 50) unexpected  
390 spectral changes take place: the intensity of the SO band decreases, accom-  
391 panied with a small blue-shift, but at the same time its high-wavenumber  
392 part, which corresponds to the vibration of the SO group of DMSO in the  
393 gas phase [87, 90] increases. This absorption band is broad and flat and its  
394 intensity increases with the DMSO dilution. In another work [89] this band  
395 was not analyzed and was probably treated as a background.

396 *3.2.2. Molecular complexes of water and DMSO – analysis of the  $\nu(S=O)$   
397 vibration bands*

398 It can be expected that fragments of DMSO linear clusters may also exist  
399 in aqueous solutions, resulting mainly from dipole–dipole interactions and  
400 the  $\text{CH}\cdots\text{O=S}$  blue-shifted hydrogen bonds. [91]. To check this hypothesis  
401 we have removed the contribution of the liquid DMSO spectrum from the  
402 measured spectra of DMSO–water mixtures shown in Fig.5a. The results are  
403 shown in Fig. 5d, which presents the corresponding dependence of the relative  
404 contribution of DMSO not forming hydrogen bonds with water. Residual  
405 spectra after this treatment (shown in Fig.S1 in the Supplementary Material)  
406 should correspond to the spectra of DMSO forming hydrogen bonds with  
407 water. Their position vs.  $x_w$  is shown in Fig. 5b. A straight line connecting

the extreme values of the band position in Fig. 5b determines the hypothetical ideal behavior of the DMSO–water solutions. It is obvious that the system is non-ideal. The inflection points of the discussed relationship suggest the existence of various molecular complexes. The first pronounced inflection point occurs at  $x_w \simeq 0.4$ , which corresponds to the  $3\text{DMSO}\cdot 2\text{H}_2\text{O}$  complex. However, such complexes are highly labile and can form many structures in the solution (see Fig.S3 in the Supplementary Material). The representative  $3\text{DMSO}\cdot 2\text{H}_2\text{O}$  complex is indicated in Fig. 4b. The next point is less marked and occurs at  $x_w \simeq 0.85$ . In this case, the stoichiometry of the complex is poorly defined and can be approximated by the set of complexes of the type  $1\text{DMSO}\cdot n\text{H}_2\text{O}$ , where  $n = 4 \div 6$ . To simplify further discussion, we will use the formula  $1\text{DMSO}\cdot 4\text{H}_2\text{O}$ , which corresponds to the core structure of the nascent hydration shell around the hydrophobic groups of DMSO. The structure of such a complex is presented in Fig. 4c. The discussed complex still lacks hydrogen bonds between water molecules around the non-polar parts of DMSO molecule. Therefore, the strong hydrogen bonds in this complex, can be attributed to the water molecules interacting with the S=O group and correspond to the population of the O···O distances characterized by the maximum at ca.  $2.75 \text{ \AA}$  in  $\Delta P(R_{OO})_{x=0.85}$ , as shown in Fig. 2b. In the discussed complex a water cage is developed around the DMSO molecule. This expansion is confirmed by DFT calculations and presented in the form of various structures in Fig. S6 in the Supplementary Material. The formation of the water cage is also evidenced from AIMD simulations which confirm (by spatial distribution functions of water oxygens around DMSO, see Fig. S11) that the particular static structures from DFT calculations indeed correlate

433 with the average solvation structure of DMSO. The last point of inflection is  
434 very sharp and corresponds to  $x_w \simeq 0.98$ .

435 It is worth noting that the distinguished solution compositions (i.e.  $x_w \simeq$   
436 0.4 and  $x_w \simeq 0.85$ ) correspond well to those observed for the HDO spectra  
437 in the range of the  $\nu(\text{OD})$  vibrations (section 3.1). Thus, changes in DMSO  
438 vibrational structure is highly correlated with changes in the arrangement of  
439 solvating water.

440 The results of the principal factor analysis (PFA algorithm) applied to  
441 the spectra in Fig. 5a lead to the conclusion that they can be adequately  
442 reproduced using four principal factors. This is also the number of absorbing  
443 species present in the solutions. By using the window factor analysis, the  
444 relative concentration profiles of these species were obtained and presented  
445 in Fig. 5c. It should be stressed that factor analysis confirmed the presence of  
446 molecular complexes in the tested solutions with compositions corresponding  
447 to the inflection points observed in Fig. 5b (black and blue). The first fac-  
448 tor corresponding to  $\nu(\text{S=O})$  band (red) shows maximum intensity for pure  
449 DMSO and can be assigned to DMSO molecules that do not form hydrogen  
450 bonds with water. As it can be seen, the dependence of the relative contri-  
451 bution of this factor vs.  $x_w$  is qualitatively similar to the one obtained in a  
452 different way and presented in Fig. 5d (red). On the other hand, the assign-  
453 ment of the factor dominant in water-rich solutions (green) requires careful  
454 consideration. Its relative contribution can be qualitatively reconstructed by  
455 a similar procedure as in the case of the first factor. For this purpose, we  
456 analyzed the participation of the boundary spectrum at  $x_w \simeq 0.98$  (with the  
457 highest intensity in Fig. 5a) in the spectra of water-rich mixtures. It must be

458 stressed, however, that this spectrum does not correspond to the infinitely  
459 diluted DMSO. It is only the closest approximation we were able to get,  
460 but the obtained contribution profile is reasonable and closely resembles the  
461 one calculated with chemometric algorithm. We attribute the fourth fac-  
462 tor (green) to DMSO molecules that are able to embed via hydrogen bonds  
463 into a clathrate-like cage of water. The corresponding relationship in Fig. 5c  
464 shows the variability of the relative proportion of DMSO molecules in this  
465 state. It should be added here that the spectra that correspond to  $x_w \gtrsim 0.98$   
466 were assigned to DMSO molecules that are partly free from hydrogen bonds  
467 within the water cage and have gained some degree of rotational freedom.

468 Molecular complexes  $3\text{DMSO}\cdot 2\text{H}_2\text{O}$  and  $1\text{DMSO}\cdot 4\text{H}_2\text{O}$  are composed of  
469 the same molecules, so it can be expected that their enthalpy of mixing will  
470 be almost ideal or close to zero. However, they differ in size and, most impor-  
471 tantly, in structure. Therefore, the non-ideality of the solution resulting from  
472 the mixing of such complexes will be reflected in the positive excess entropy,  
473 in accordance with the theory of athermal solutions developed by Huggins  
474 [92], Flory [93] and Miller [94]. Hence, a solution with a composition cor-  
475 responding to equal relative contributions of both complexes, corresponding  
476 to  $x_w = 0.67$  (marked with the red dashed line in Fig. 5c) should have the  
477 maximum entropy. This, in turn, translates into the minimum of the Gibbs  
478 free energy of such solution. Finally, it should consequently have a mini-  
479 mum temperature of solidification. In our opinion, the presented reasoning  
480 explains the occurrence of an eutectic point for the DMSO–water system at  
481  $x_w = 0.67$ . Its appearance is thus of entropic nature and corresponds to the  
482 largest number of configurations responsible for the intermolecular interac-

tions between the highlighted molecular complexes. Previously, Kircher and Reiher [31] proposed a somewhat similar concept. Accordingly, in the eutectic mixture many energetically similar, but structurally different molecular complexes exist (proposed by the authors on the basis of *ab initio* calculations) that cannot easily transform their conformations into one another. It leads to the hindered formation of hydrogen bonds between clusters. We want to emphasize that on the basis of our results we see no premise for the existence of the  $1\text{DMSO}\cdot 2\text{H}_2\text{O}$  molecular complex, often postulated by other authors (ref. [25] and references cited therein), which would justify the depression of melting point of the solutions at the discussed composition.

#### 3.2.3. Spectra in the range of $\nu(\text{C-H})$ vibrations

The asymmetric and symmetric  $\nu(\text{C-H})$  bands of DMSO methyl groups (located at  $2996 \pm 1$  and  $2912 \pm 1\text{ cm}^{-1}$ , respectively, in the case of pure DMSO; data not shown) demonstrate a clear blue-shift of 22 and  $12\text{ cm}^{-1}$ , respectively, as the water content in mixtures with DMSO increases. Such a shift corresponds to the formation of hydrogen bonds of the  $\text{C-H}\cdots\text{OH}_2$  type between methyl groups of DMSO and lone electron pairs of water molecules [31, 95, 96, 97, 98, 99, 100]. The rate of the shift with increasing  $x_w$  clearly accelerates after exceeding  $x_w \simeq 0.5$ . The corresponding dependencies of the band shift on  $x_w$  can be found in previous works [95, 100]. It is important to note the change of the blue-shift into the red-shift for  $x_w > 0.96$ . We can associate this unexpected change in the direction of the band shift with the already discussed change of the behavior of the  $\nu(\text{S=O})$  band in a very similar range of compositions. Clearly, relatively weak hydrogen bonds of the  $\text{C-H}\cdots\text{OH}_2$  type, which are two to four times weaker than water–water

508 hydrogen bonds [31, 97, 99], play a special or even a key role in the in-  
509 termolecular interactions between DMSO and water. The high importance  
510 of such hydrogen bonds, disregarding their relatively weak character, stems  
511 from their non-negligible number: the analysis of AIMD simulations shows  
512 that almost 0.5 hydrogen bonds per C-H bond, and simultaneously 2.5 such  
513 bonds per DMSO molecule, are formed on average (see Figs. S8 and S9 in  
514 the Supplementary Material).

515 The role of C-H $\cdots$ OH<sub>2</sub> “improper” hydrogen bonds becomes clear when  
516 the RDG method is applied to the electron densities calculated for DFT-  
517 optimized complexes of DMSO with different number of surrounding water  
518 molecules (including both low—classical DFT—and high—ONIOM-based—  
519 water content complexes). Such bonds are weaker than other hydrogen  
520 bonds, yet their orientation and localization between the hydrogen bond  
521 donor and acceptor are as good (Fig. 4). These bonds are present even in pure  
522 DMSO complexes and facilitate the self-association of molecules (Fig. 4a).  
523 When water molecules are introduced into the complex, such interactions be-  
524 come possible also between the oxygen atom of water molecules and methyl  
525 groups of DMSO (Fig. 4b). However, the most important role of such bond-  
526 ing is clearly visible when the number of water molecules is high enough to  
527 form an initial core structure of the future hydration shell (Fig. 4c). These  
528 hydrogen bonds impose the position of water molecules and stabilize the  
529 shell formation. The core is stabilized solely by proper and improper hydro-  
530 gen bonds, and the van der Waals interactions are almost absent, even with  
531 10 water molecules per one DMSO (Fig. 6a). These interactions, however,  
532 tend to substitute C-H $\cdots$ OH<sub>2</sub> bonds when the number of water molecules is

533 high enough to almost cover one of the methyl groups, as in Fig. 6b. In this  
534 figure, two “improper” bonds are visible around the left CH<sub>3</sub> group, while  
535 the right one interacts with its hydration shell through van der Waals in-  
536 teractions marked with green/olive flat surfaces. In complexes with higher  
537 water content the, “improper” hydrogen bonds are almost absent and the  
538 hydrophobic part of the DMSO molecule is covered with patches of van der  
539 Waals interactions (Fig. 6c).

540 ——Figure 6——

541 The change in the character of DMSO–water interactions is reflected also  
542 in the simple geometry of ONIOM-calculated complexes. When the hydra-  
543 tion shell starts to cover the central DMSO molecule, more and more C–H  
544 bonds are released from the “improper” hydrogen bonds. Consequently, the  
545 mean C–H bond length is shortened (Fig. S4 in Supplementary Material),  
546 which translates into the blue-shift observed in the FTIR spectra. The pro-  
547 cess is stopped when the hydration shell is complete and such hydrogen bonds  
548 are no more present in the complexes. We note here that the complete hy-  
549 dration shell of DMSO at  $x_w \simeq 0.988$  (the AIMD-studied system) contains  
550 on average 29.2 water molecules (see Fig. S10 and Table S2 in the Supple-  
551 mentary Material). The C–H bond length reaches minimum at ca. 30 water  
552 molecules per 1 DMSO and increases at higher water contents. We note  
553 here that this closely corresponds to the number of water molecules in the  
554 full hydration shell of DMSO, as evidenced by DMSO···D<sub>2</sub>O radial distribu-  
555 tion function obtained from AIMD simulations (see Fig. S10 and Table S2  
556 in Supplementary Material). Moreover, the mean C<sub>DMSO</sub>···O<sub>water</sub> distance  
557 increases with the number of water molecules in the shell (Fig. S5 in Supple-

558      mentary Material). Such geometry change of the water cage around DMSO  
559      favors partial rotational freedom of the guest molecule inside, as suggested by  
560      FTIR spectra of DMSO in the range of  $\nu(\text{S=O})$  vibrations (see also section  
561      3.2.1).

562      *3.2.4. Increase of the rotational freedom of DMSO molecule in its water cage*

563      It seems very likely that hydrogen bonding of the red-shifted and the blue-  
564      shifted types are cooperative according to refs [98, 99, 100]. It is also possible  
565      that DMSO is not an exception and other solutes, including biomolecules,  
566      can undergo a similar process. The way of formation of the hydration cage  
567      is generally consistent with the progressive hydration model proposed by  
568      Mrázkowá and Hobza [97]. The only caveat resulting from our research  
569      concerns the fact that the blue-shifted hydrogen bonds become less important  
570      when the construction of the water cage becomes fully complete and the cage  
571      itself becomes more relaxed.

572      The aforementioned weakening of the water hydrogen bonds with the  
573       $\text{S=O}$  group of DMSO (section 3.2.1), progressing with the increasing size  
574      of the hydration complex, together with changes in the interaction of the  
575      water cage with DMSO molecule and the modification of the size of the cage  
576      itself (inferred from the DFT calculations presented in section 3.2.3) create  
577      conditions for the partial release of the DMSO molecule from the network  
578      of hydrogen bonds with water to a degree that allows a certain rotational  
579      freedom. This is supported by the spectral effects observed in Fig. 5a (blue  
580      lines) and the change of the blue-shift into the red-shift of the  $\nu(\text{C-H})$  DMSO  
581      bands [95, 100] taking place at the lowest DMSO concentrations. The driving  
582      force behind the observed phenomenon is the entropy gain associated with

583 the recovery of rotational freedom of the guest molecule.

584 We also note here that the formation of the water cage is connected with  
585 the orientational retardation of water molecules in the DMSO hydration shell,  
586 as clearly evidenced by the orientational relaxation time of the O–D bond of  
587  $\text{D}_2\text{O}$  increasing from 2.3 ps in bulk water to 3.1 ps in the hydration shell, see  
588 the Supplementary Material for details.

589 *3.3. Hydration of DMSO in the light of other water-soluble solutes regarded  
590 as “hydrophobic”*

591 Recently, Grdadolnik *et al.* [13] have demonstrated, the presence of  
592 the ice-like hydration water around small purely hydrophobic solutes (i.e.,  
593 methane, ethane, krypton, and xenon). Ice (Ih), solid clathrates of these  
594 substances and their solutions gave a single  $\nu(\text{OD})$  band of HDO at the same  
595 position, ca.  $2440 \pm 10 \text{ cm}^{-1}$ , which corresponds to  $R_{\text{OO}} = 2.76 \pm 0.01 \text{ \AA}$ .

596 —Figure 7—

597 Substances included in Fig. 7 allow us to better justify the thesis that the  
598 hydration of DMSO in water-rich solutions is hydrophobic in nature, leading  
599 to the formation of a clathrate-like structure. Both the tetrabutylammonium  
600 cation ( $\text{Bu}_4\text{N}^+$ ) and tetrahydrofuran (THF) form solid clathrates [103, 104,  
601 105] and are commonly regarded as model hydrophobic molecules [105, 106,  
602 44, 101]. The hydration sphere in both cases is composed of ice-like water  
603 molecules and the accompanying population of water molecules with  $\text{O}\cdots\text{O}$   
604 distances longer than in the bulk water. The latter often dominates and  
605 obscures the effect of the presence of “ice-like” water molecules [79]. However,  
606 among the solutes listed in Fig. 7, DMSO is characterized by a hydration  
607 sphere in which water molecules with the “ice-like” structure are dominant

608 ( $R_{OO} \simeq 2.75 \text{ \AA}$ ).

609 The use of differences between interatomic O···O distance distribution  
610 functions (Fig. 7b) is probably the most appropriate method for uncovering  
611 the presence of subtle and labile structures in solution. Simulation methods  
612 can also sometimes fail in this respect if we take into account the information  
613 resulting from the analysis of the affected spectra, regarding the affected  
614 number,  $N$  (note, however, that the normalization factor for the distance-  
615 dependent IR spectra derived from AIMD simulations often remains in close  
616 correspondence to the experimental  $N$  value, as found also in this work).

617 It can be estimated on the basis of Fig. 7b that within the hydration  
618 sphere of DMSO the contribution of “ice-like” water ( $R_{OO} \simeq 2.75 \text{ \AA}$ ) relative  
619 to the water with a weakened structure ( $R_{OO} \simeq 2.90 \text{ \AA}$ ) is close to 2/3. Tak-  
620 ing into account the  $N$  value for the infinite dilution solution (2.8, see inset  
621 in Fig. 2a and Table S1 in Supplementary Material), we obtain ca. 2 wa-  
622 ter molecules which statistically form the ice-like structure in the hydration  
623 sphere of DMSO. However, we must take into account that about half of this  
624 population are water molecules that form hydrogen bonds with the DMSO  
625 oxygen atom (Fig. 2b). On the other hand, for  $\text{Bu}_4\text{N}^+$  it can be estimated,  
626 basing on data in ref. [44], that  $N$  equals to ca. 3 and that the contribution  
627 of the “ice-like” water in the cation hydration sphere is close to 1/3 (Fig. 7),  
628 which indicates that statistically only 1 water molecule of the “ice-like” struc-  
629 ture can be found in its hydration sphere. As it can be seen in Fig. 7b, THF  
630 ( $N = 3.2$  [101]) lies between DMSO and  $\text{Bu}_4\text{N}^+$  in respect of proportion  
631 of the “ice-like” water and the water with weakened structure. Therefore,  
632 for typical water-soluble small solutes that contain non-polar groups one can

633 expect on average one water molecule forming the “ice-like” structure.

634 In the light of the above-mentioned Grdadolnik’s findings [13], the ques-  
635 tion arises about the origin of the accompanying population of water molecules  
636 with weakened hydrogen bonding in the case of hydrophobic water-soluble  
637 molecules. The formal answer to this question arises from simple thermody-  
638 namic predictions. Because the formation of the “iceberg”, triggered by the  
639 presence of the solute, is very entropy consuming and leads to a low solubility  
640 of such solute, any other structural opportunity for water molecules which  
641 is less “structured” will be more thermodynamically favorable and improve  
642 the solubility in water. An explanation on the molecular level should take  
643 into account also molecular premises. It should be noted that in the case of  
644  $\text{Bu}_4\text{N}^+$  cation the solvent accessible surface consists of convex and concave  
645 areas. Water molecules in the surroundings of the convex area have a chance  
646 to build a network of ice-type hydrogen bonds with an approximately parallel  
647 molecule orientation relative to the surface. On the other hand, in the con-  
648 cave areas the probability of perpendicular orientation of water molecules,  
649 i.e. with their lone electron pairs pointing towards the hydrophobic surface,  
650 is growing. As has been discussed in the Supplementary Material (section  
651 S1.3), water molecules which do not engage their lone electron pairs in clas-  
652 sical hydrogen bonds are less polarized and exhibit a blue-shifted  $\nu(\text{OD}/\text{OH})$   
653 band. According to this argumentation, those water molecules which are in  
654 the concave areas of the  $\text{Bu}_4\text{N}^+$  cation should contribute to the population of  
655 molecules with “weakened hydrogen bonds”. Those molecules which are in  
656 the vicinity of convex areas should contribute to the population of the  
657 ice-like water molecules. In the case of DMSO, the accompanying population

658 of molecules with weakened hydrogen bonds originate from improper fit of  
659 water molecules hydrogen bonded to the oxygen atom of DMSO, to the bulk  
660 water, as recognized in this work from AIMD simulations. In the case of  
661 THF hydration, it can be presumed that the source of water molecules with  
662 weakened hydrogen bonds is similar in nature to the DMSO case.

663 **4. Conclusions**

664 DMSO-water mixtures have been studied by means of the FTIR spec-  
665 troscopy in the range of DMSO vibration and HDO stretching vibrations  
666 (as a probe of hydration water) in the whole range of mixture compositions.  
667 Theoretical calculations facilitated the interpretation of experimental results.  
668 This helped us to redefine the view on the hydration of DMSO.

669 It has been established that in diluted solutions of DMSO the clathrate-  
670 like water cage is created around the DMSO molecule. The formation of  
671 this cage is facilitated by interactions between water molecules and methyl  
672 groups of the guest molecule (the blue-shifted hydrogen bonds) and it is  
673 particularly evidenced by the spatial distribution function of water around  
674 DMSO that clearly displays the emergence of cage structures around methyl  
675 groups. For even more diluted solutions, when the water cage is fully com-  
676 pleted, the DMSO molecule partly regains its rotational freedom inside. The  
677 driving force behind this effect is the entropy gain. Weakened hydrogen  
678 bonds of water molecules population arise from those water molecules which  
679 are hydrogen bonded to the ones already interacting with the oxygen atom of  
680 DMSO. Most probably, it happens because strong hydrogen bonds of water  
681 molecules directly bonded to the hydrophilic group of the solute poorly fit

to the structure of the bulk water. This population with weakened hydrogen bonds efficiently obscures the presence of the population with strong hydrogen bonds formed with the SO group of DMSO and between water molecules around the methyl groups in the overall spectral effect. We also propose a novel explanation of the strong deviation from ideality of DMSO-water mixtures at composition corresponding to the eutectic point of the system. Namely, it stems from an equimolar mixture of the molecular complexes of the  $3\text{DMSO}\cdot 2\text{H}_2\text{O}$  and of  $1\text{DMSO}\cdot n\text{H}_2\text{O}$  ( $n = 4 \div 6$ ) type. For such a mixing the, maximum excess entropy is expected, which justifies the depression of the melting point of the solution at  $x_w = 0.67$ .

## 5. Acknowledgements

J. S. would like to thank Dr. Ewa Kamieńska-Piotrowicz for her help in experiment. Calculations were carried out at the Academic Computer Centre in Gdańsk.

## 6. Declaration of interest

The authors declare that they have no conflict of interest.

[1] P. Ball, Water is an active matrix of life for cell and molecular biology., Proceedings of the National Academy of Sciences of the United States of America 114 (2017) 13327–13335.

[2] W. Kauzmann, Some Factors in the Interpretation of Protein Denaturation, Advances in Protein Chemistry 14 (1959) 1–63.

- 703 [3] C. Tanford, The hydrophobic effect and living matter, *Science* 200  
704 (1978) 1012–1018.
- 705 [4] M. Charton, B. I. Charton, The structural dependence of amino acid  
706 hydrophobicity parameters, *Journal of Theoretical Biology* 99 (1982)  
707 629–644.
- 708 [5] R. L. Baldwin, Temperature dependence of the hydrophobic interaction  
709 in protein folding., *Proceedings of the National Academy of Sciences*  
710 83 (1986) 8069–8072.
- 711 [6] K. A. Dill, Dominant forces in protein folding, *Biochemistry* 29 (1990)  
712 7133–7155.
- 713 [7] W. Blokzijl, J. B. Engberts, Hydrophobic Effects. Opinions and Facts,  
714 *Angewandte Chemie International Edition in English* 32 (1993) 1545–  
715 1579.
- 716 [8] V. R. Agashe, M. C. R. Shastry, J. B. Udgaonkar, Initial hydrophobic  
717 collapse in the folding of barstar, *Nature* 377 (1995) 754–757.
- 718 [9] H. J. Dyson, P. E. Wright, H. A. Scheraga, The role of hydrophobic in-  
719 teractions in initiation and propagation of protein folding, *Proceedings*  
720 *of the National Academy of Sciences* 103 (2006) 13057–13061.
- 721 [10] P. Ball, Water as an Active Constituent in Cell Biology, *Chemical*  
722 *Reviews* 108 (2008) 74–108.
- 723 [11] H. S. Frank, M. W. Evans, Free Volume and Entropy in Condensed  
724 Systems III. Entropy in Binary Liquid Mixtures; Partial Molal En-

- 725       tropy in Dilute Solutions; Structure and Thermodynamics in Aqueous  
726       Electrolytes, *The Journal of Chemical Physics* 13 (1945) 507–532.
- 727       [12] T. Hajari, S. Bandyopadhyay, Water structure around hydrophobic  
728       amino acid side chain analogs using different water models, *The Journal*  
729       of *Chemical Physics* 146 (2017) 225104.
- 730       [13] J. Grdadolnik, F. Merzel, F. Avbelj, Origin of hydrophobicity and en-  
731       hanced water hydrogen bond strength near purely hydrophobic solutes,  
732       *Proceedings of the National Academy of Sciences* 114 (2017) 322–327.
- 733       [14] D. T. Bowron, A. Filippini, M. A. Roberts, J. L. Finney, Hydrophobic  
734       Hydration and the Formation of a Clathrate Hydrate, *Physical Review*  
735       Letters 81 (1998) 4164–4167.
- 736       [15] N. Uras-Aytemiz, I. Abrrey Montreal, J. P. Devlin, Communication:  
737       Quantitative Fourier-transform infrared data for competitive loading  
738       of small cages during all-vapor instantaneous formation of gas-hydrate  
739       aerosols, *Journal of Chemical Physics* 135 (2011) 2–5.
- 740       [16] J. L. Finney, Overview lecture. Hydration processes in biological and  
741       macromolecular systems, *Faraday Discussions* 103 (1996) 1.
- 742       [17] A. K. Soper, Neutron scattering studies of solvent structure in systems  
743       of chemical and biological importance, *Faraday Discussions* 103 (1996)  
744       41.
- 745       [18] D. Martin, A. Weise, H.-J. Niclas, The Solvent Dimethyl Sulfoxide,  
746       *Angewandte Chemie International Edition in English* 6 (1967) 318–  
747       334.

- 748 [19] U. Kaatze, R. Pottel, M. Schaefer, Dielectric spectrum of dimethyl  
749 sulfoxide/water mixtures as a function of composition, *The Journal of*  
750 *Physical Chemistry* 93 (1989) 5623–5627.
- 751 [20] Z. Lu, E. Manias, M. Lanagan, D. Macdonald, Dielectric Relaxation  
752 in Dimethyl Sulfoxide/Water Mixtures, *ECS Transactions* 28 (2010)  
753 11–21.
- 754 [21] S. Y. Lam, R. L. Benoit, Some Thermodynamic Properties of the  
755 Dimethylsulfoxide–Water and Propylene Carbonate–Water Systems at  
756 25°C, *Canadian Journal of Chemistry* 52 (1974) 718–722.
- 757 [22] J. T. Cabral, A. Luzar, J. Teixeira, M.-C. Bellissent-Funel, Single-  
758 particle dynamics in dimethyl-sulfoxide/water eutectic mixture by neu-  
759 tron scattering, *The Journal of Chemical Physics* 113 (2000) 8736.
- 760 [23] I. A. Borin, M. S. Skaf, Molecular association between water and  
761 dimethyl sulfoxide in solution: A molecular dynamics simulation study,  
762 *The Journal of Chemical Physics* 110 (1999) 6412–6420.
- 763 [24] P. P. Wiewiór, H. Shirota, E. W. Castner, Aqueous dimethyl sulfox-  
764 ide solutions: Inter- and intra-molecular dynamics, *The Journal of*  
765 *Chemical Physics* 116 (2002) 4643–4654.
- 766 [25] V. M. Wallace, N. R. Dhumal, F. M. Zehentbauer, H. J. Kim,  
767 J. Kiefer, Revisiting the Aqueous Solutions of Dimethyl Sulfoxide  
768 by Spectroscopy in the Mid- and Near-Infrared: Experiments and  
769 Car–Parrinello Simulations, *The Journal of Physical Chemistry B* 119  
770 (2015) 14780–14789.

- 771 [26] J. M. G. Cowie, P. M. Toporowski, Association in the binary liquid  
772 system dimethyl sulphoxide-water, Canadian Journal of Chemistry 39  
773 (1961) 2240–2243.
- 774 [27] S. S. N. Murthy, Phase Behavior of the Supercooled Aqueous Solu-  
775 tions of Dimethyl Sulfoxide, Ethylene Glycol, and Methanol As Seen  
776 by Dielectric Spectroscopy, The Journal of Physical Chemistry B 101  
777 (1997) 6043–6049.
- 778 [28] I. I. Vaisman, M. L. Berkowitz, Local structural order and molecu-  
779 lar associations in water-DMSO mixtures. Molecular dynamics study,  
780 Journal of the American Chemical Society 114 (1992) 7889–7896.
- 781 [29] I. A. Borin, M. S. Skaf, Molecular association between water and  
782 dimethyl sulfoxide in solution: the librational dynamics of water,  
783 Chemical Physics Letters 296 (1998) 125–130.
- 784 [30] A. Vishnyakov, A. P. Lyubartsev, A. Laaksonen, Molecular Dynam-  
785 ics Simulations of Dimethyl Sulfoxide and Dimethyl Sulfoxide-Water  
786 Mixture, The Journal of Physical Chemistry A 105 (2001) 1702–1710.
- 787 [31] B. Kirchner, M. Reiher, The Secret of Dimethyl Sulfoxide-Water Mix-  
788 tures. A Quantum Chemical Study of 1DMSO- n Water Clusters, Jour-  
789 nal of the American Chemical Society 124 (2002) 6206–6215.
- 790 [32] G. J. Safford, P. C. Schaffer, P. S. Leung, G. F. Doeblner, G. W. Brady,  
791 E. F. X. Lyden, Neutron Inelastic Scattering and X-Ray Studies of  
792 Aqueous Solutions of Dimethylsulphoxide and Dimethylsulphone, The  
793 Journal of Chemical Physics 50 (1969) 2140–2159.

- 794 [33] D. H. Rasmussen, A. P. MacKenzie, Phase Diagram for the System  
795 Water–Dimethylsulphoxide, *Nature* 220 (1968) 1315–1317.
- 796 [34] E. S. Baker, J. Jonas, Transport and relaxation properties of dimethyl  
797 sulfoxide-water mixtures at high pressure, *The Journal of Physical  
798 Chemistry* 89 (1985) 1730–1735.
- 799 [35] A. K. Soper, A. Luzar, Orientation of Water Molecules around Small  
800 Polar and Nonpolar Groups in Solution: A Neutron Diffraction and  
801 Computer Simulation Study, *The Journal of Physical Chemistry* 100  
802 (1996) 1357–1367.
- 803 [36] Y. Koga, Y. Kasahara, K. Yoshino, K. Nishikawa, Mixing Schemes  
804 for Aqueous Dimethyl Sulfoxide: Support by X-ray Diffraction Data,  
805 *Journal of Solution Chemistry* 30 (2001) 885–893.
- 806 [37] Z. S. Klemenkova, E. G. Kononova, Elucidation of the Water–DMSO  
807 Mixing Process Based on an IR Study, *Journal of Solution Chemistry*  
808 44 (2015) 280–292.
- 809 [38] R. L. Mancera, M. Chalaris, K. Refson, J. Samios, Molecular dy-  
810 namics simulation of dilute aqueous DMSO solutions. A temperature-  
811 dependence study of the hydrophobic and hydrophilic behaviour  
812 around DMSO, *Physical Chemistry Chemical Physics* 6 (2004) 94.
- 813 [39] R. L. Mancera, M. Chalaris, J. Samios, The concentration effect on  
814 the ‘hydrophobic’ and ‘hydrophilic’ behaviour around DMSO in dilute  
815 aqueous DMSO solutions. A computer simulation study, *Journal of  
816 Molecular Liquids* 110 (2004) 147–153.

- 817 [40] K. Subbarangaiah, N. M. Murthy, S. V. Subrahmanyam, Ultrasonic Investigation on the Structure of Aqueous Solutions of *N,N*-  
818 Dimethylformamide and Dimethyl Sulfoxide, Bulletin of the Chemical  
819 Society of Japan 54 (1981) 2200–2204.
- 820
- 821 [41] G. Petrella, M. Petrella, M. Castagnolo, A. Dell'Atti, A. De Giglio,  
822 Solute-Solvent interactions in water-rich mixtures. II. Ionic conductances in water-dimethylsulfoxide mixtures at 25°C, Journal of Solution  
823 Chemistry 10 (1981) 129–138.
- 824
- 825 [42] A. Panuszko, P. Bruździak, E. Kaczkowska, J. Stangret, General Mechanism of Osmolytes' Influence on Protein Stability Irrespective of the  
826 Type of Osmolyte Cosolvent, The Journal of Physical Chemistry B  
827 120 (2016) 11159–11169.
- 828
- 829 [43] J. Stangret, Solute-Affected Vibrational Spectra of Water in Ca(ClO<sub>4</sub>)<sub>2</sub>  
830 Aqueous Solutions, Spectroscopy Letters 21 (1988) 369–381.
- 831
- 832 [44] J. Stangret, T. Gampe, Hydration Sphere of Tetrabutylammonium Cation. FTIR Studies of HDO Spectra, The Journal of Physical Chemistry B  
833 103 (1999) 3778–3783.
- 834
- 835 [45] M. Śmiechowski, J. Stangret, Vibrational spectroscopy of semiheavy water (HDO) as a probe of solute hydration, Pure and Applied Chemistry  
836 82 (2010) 1869–1887.
- 837
- 838 [46] E. Malinowski, Factor Analysis in Chemistry, Wiley, New York, 2002.  
[47] E. R. Malinowski, Window factor analysis: Theoretical derivation and

839 application to flow injection analysis data, *Journal of Chemometrics* 6  
840 (1992) 29–40.

- 841 [48] M. J. Frisch, G. W. Trucks, H. B. Schlegel, G. E. Scuseria, M. A.  
842 Robb, J. R. Cheeseman, G. Scalmani, V. Barone, B. Mennucci, G. A.  
843 Petersson, H. Nakatsuji, M. Caricato, X. Li, H. P. Hratchian, A. F.  
844 Izmaylov, J. Bloino, G. Zheng, J. L. Sonnenberg, M. Hada, M. Ehara,  
845 K. Toyota, R. Fukuda, J. Hasegawa, M. Ishida, T. Nakajima, Y. Honda,  
846 O. Kitao, H. Nakai, T. Vreven, J. A. Montgomery Jr., J. E. Peralta,  
847 F. Ogliaro, M. Bearpark, J. J. Heyd, E. Brothers, K. N. Kudin, V. N.  
848 Staroverov, R. Kobayashi, J. Normand, K. Raghavachari, A. Rendell,  
849 J. C. Burant, S. S. Iyengar, J. Tomasi, M. Cossi, N. Rega, J. M. Millam,  
850 M. Klene, J. E. Knox, J. B. Cross, V. Bakken, C. Adamo, J. Jaramillo,  
851 R. Gomperts, R. E. Stratmann, O. Yazyev, A. J. Austin, R. Cammi,  
852 C. Pomelli, J. W. Ochterski, R. L. Martin, K. Morokuma, V. G. Za-  
853 krzewski, G. A. Voth, P. Salvador, J. J. Dannenberg, S. Dapprich, A. D.  
854 Daniels, Ö. Farkas, J. B. Foresman, J. V. Ortiz, J. Cioslowski, D. J.  
855 Fox, *Gaussian 09*, Revision D.01, 2009.
- 856 [49] E. R. Johnson, S. Keinan, P. Mori-Sanchez, J. Contreras-Garcia, A. J.  
857 Cohen, W. Yang, Revealing noncovalent interactions, *Journal of the  
858 American Chemical Society* 132 (2010) 6498–6506.
- 859 [50] T. Lu, F. Chen, Multiwfn: A multifunctional wavefunction analyzer,  
860 *Journal of Computational Chemistry* 33 (2012) 580–592.
- 861 [51] S. Grimme, S. Ehrlich, L. Goerigk, Effect of the damping function in

- 862 dispersion corrected density functional theory, Journal of Computational  
863 Chemistry 32 (2011) 1456–1465.
- 864 [52] C. Lee, W. Yang, R. G. Parr, Development of the Colle-Salvetti  
865 correlation-energy formula into a functional of the electron density,  
866 Phys. Rev. B 37 (1988) 785–789.
- 867 [53] A. D. Becke, Density-functional thermochemistry. III. the role of exact  
868 exchange, The Journal of Chemical Physics 98 (1993) 5648–5652.
- 869 [54] R. Ditchfield, W. J. Hehre, J. A. Pople, Self-consistent molecular-  
870 orbital methods. IX. an extended gaussian-type basis for molecular-  
871 orbital studies of organic molecules, The Journal of Chemical Physics  
872 54 (1971) 724–728.
- 873 [55] V. Barone, M. Cossi, Quantum calculation of molecular energies and  
874 energy gradients in solution by a conductor solvent model, Journal of  
875 Physical Chemistry A 102 (1998) 1995–2001.
- 876 [56] M. Cossi, N. Rega, G. Scalmani, V. Barone, Energies, structures, and  
877 electronic properties of molecules in solution with the C-PCM solvation  
878 model, Journal of Computational Chemistry 24 (2003) 669–681.
- 879 [57] V. P. Ananikov, D. G. Musaev, K. Morokuma, Real size of ligands,  
880 reactants and catalysts: Studies of structure, reactivity and selectivity  
881 by ONIOM and other hybrid computational approaches, Journal of  
882 Molecular Catalysis A: Chemical 324 (2010) 104–119.

- 883 [58] T. A. Halgren, Merck molecular force field. I. Basis, form, scope, pa-  
884 rameterization, and performance of MMFF94, *J. Comput. Chem.* 17  
885 (1996) 490–519.
- 886 [59] T. A. Halgren, Merck molecular force field. II. MMFF94 van der Waals  
887 and electrostatic parameters for intermolecular interactions, *J. Com-  
888 put. Chem.* 17 (1996) 520–552.
- 889 [60] D. Marx, J. Hutter, *Ab Initio Molecular Dynamics*, Cambridge Uni-  
890 versity Press, Cambridge, 2009.
- 891 [61] J. VandeVondele, M. Krack, F. Mohamed, M. Parrinello, T. Chassaing,  
892 J. Hutter, Quickstep: Fast and accurate density functional calculations  
893 using a mixed Gaussian and plane waves approach, *Computer Physics  
894 Communications* 167 (2005) 103–128.
- 895 [62] The cp2k Developers Group, cp2k v. 6.0, 2001–2018.  
896 <http://www.cp2k.org/>.
- 897 [63] J. Hutter, M. Iannuzzi, F. Schiffmann, J. VandeVondele, cp2k: atom-  
898 istic simulations of condensed matter systems, *WIREs Comput. Mol.  
899 Sci.* 4 (2014) 15–25.
- 900 [64] A. D. Becke, Density-functional exchange-energy approximation with  
901 correct asymptotic behavior, *Phys. Rev. A* 38 (1988) 3098–3100.
- 902 [65] S. Grimme, J. Antony, S. Ehrlich, H. Krieg, A consistent and accurate  
903 *ab initio* parametrization of density functional dispersion correction  
904 (DFT-D) for the 94 elements H-Pu, *J. Chem. Phys.* 132 (2010) 154104.

- 905 [66] G. Lippert, J. Hutter, M. Parrinello, A hybrid Gaussian and plane  
906 wave density functional scheme, Mol. Phys. 92 (1997) 477–487.
- 907 [67] S. Goedecker, M. Teter, J. Hutter, Separable dual-space Gaussian  
908 pseudopotentials, Phys. Rev. B 54 (1996) 1703–1710.
- 909 [68] M. Nakamura, K. Tamura, S. Murakami, Isotope effects on thermody-  
910 namic properties: mixtures of  $x(D_2O$  or  $H_2O) + (1-x)CH_3CN$  at 298.15  
911 K, Thermochim. Acta 253 (1995) 127–136.
- 912 [69] R. B. Torres, P. L. O. V. A. C. M. Marchiore, Volumetric properties  
913 of binary mixtures of (water + organic solvents) at temperatures be-  
914 tween  $T = 288.15$  K and  $T = 303.15$  K at  $p = 0.1$  MPa, J. Chem.  
915 Thermodynamics 38 (2006) 526–541.
- 916 [70] I.-F. W. Kuo, C. J. Mundy, M. J. McGrath, J. I. Siepmann, J. Van-  
917 deVondele, M. Sprik, J. Hutter, B. Chen, M. L. Klein, F. Mohamed,  
918 M. Krack, M. Parrinello, Liquid Water from First Principles: Investi-  
919 gation of Different Sampling Approaches, J. Phys. Chem. B 108 (2004)  
920 12990–12998.
- 921 [71] T. Bryk, A. P. Seitsonen, Ab initio molecular dynamics study of collec-  
922 tive excitations in liquid  $H_2O$  and  $D_2O$ : Effect of dispersion corrections,  
923 Condens. Matter Phys. 19 (2016) 1–14.
- 924 [72] G. J. Martyna, M. L. Klein, M. Tuckerman, Nosé–Hoover chains: The  
925 canonical ensemble via continuous dynamics, J. Chem. Phys. 97 (1992)  
926 2635–2643.

- 927 [73] N. Marzari, D. Vanderbilt, Maximally localized generalized Wannier  
928 functions for composite energy bands, Phys. Rev. B 56 (1997) 12847–  
929 12865.
- 930 [74] M. Thomas, M. Brehm, R. Fligg, P. Vöringer, B. Kirchner, Computing  
931 vibrational spectra from ab initio molecular dynamics, Phys. Chem. Chem.  
932 Phys. Chem. Phys. 15 (2013) 6608–6622.
- 933 [75] M. Śmiechowski, J. Sun, H. Forbert, D. Marx, Solvation shell resolved  
934 THz spectra of simple aqua ions – distinct distance- and frequency-  
935 dependent contributions of solvation shells, Phys. Chem. Chem. Phys.  
936 17 (2015) 8323–8329.
- 937 [76] M. Śmiechowski, Unusual Influence of the Fluorinated Anions on the  
938 Stretching Vibrations of Liquid Water, J. Phys. Chem. B 122 (2018)  
939 3141–3152.
- 940 [77] H. Odhner, D. T. Jacobs, Refractive Index of Liquid D<sub>2</sub>O for Visible  
941 Wavelengths, J. Chem. Eng. Data 57 (2012) 166–168.
- 942 [78] J. Stangret, Donor properties of water in organic solvents derived from  
943 infrared spectra of HDO, Journal of Molecular Structure 643 (2002)  
944 29–35.
- 945 [79] E. Gojło, T. Gampe, J. Krakowiak, J. Stangret, Hydration of Aprotic  
946 Donor Solvents Studied by Means of FTIR Spectroscopy, The Journal  
947 of Physical Chemistry A 111 (2007) 1827–1834.
- 948 [80] J. E. Bertie, M. K. Ahmed, H. H. Eysel, Infrared intensities of liquids.  
949 5. Optical and dielectric constants, integrated intensities, and dipole

- 950 moment derivatives of H<sub>2</sub>O and D<sub>2</sub>O at 22 °C, J. Phys. Chem. 93  
951 (1989) 2210–2218.
- 952 [81] M. Heyden, J. Sun, S. Funkner, G. Mathias, H. Forbert, M. Havenith,  
953 D. Marx, Dissecting the THz spectrum of liquid water from first prin-  
954 ciples via correlations in time and space, Proc. Natl. Acad. Sci. USA  
955 107 (2010) 12068–12073.
- 956 [82] L. R. Pestana, N. Mardirossian, M. Head-Gordon, T. Head-Gordon,  
957 Ab initio molecular dynamics simulations of liquid water using high  
958 quality meta-GGA functionals, Chem. Sci. 8 (2017) 3554–3565.
- 959 [83] O. Marsalek, T. E. Markland, Quantum Dynamics and Spectroscopy  
960 of Ab Initio Liquid Water: The Interplay of Nuclear and Electronic  
961 Quantum Effects, J. Phys. Chem. Lett. 8 (2017) 1545–1551.
- 962 [84] M. Leśniewski, M. Śmiechowski, Communication: Inside the water  
963 wheel: Intrinsic differences between hydrated tetraphenylphosphonium  
964 and tetraphenylborate ions, J. Chem. Phys. 149 (2018) 171101.
- 965 [85] S. Imoto, H. Forbert, D. Marx, Aqueous TMAO solutions as seen by  
966 theoretical THz spectroscopy: hydrophilic versus hydrophobic water,  
967 Phys. Chem. Chem. Phys. 20 (2018) 6146–6158.
- 968 [86] W. N. Martens, R. L. Frost, J. Kristof, J. Theo Kloprogge, Raman  
969 spectroscopy of dimethyl sulphoxide and deuterated dimethyl sulphox-  
970 ide at 298 and 77 K, Journal of Raman Spectroscopy 33 (2002) 84–91.
- 971 [87] M.-T. Forel, M. Tranquille, Spectres de vibration du diméthylsulfoxyde

- et dn diméthylsulfoxyde-d6, Spectrochimica Acta Part A: Molecular Spectroscopy 26 (1970) 1023–1034.
- [88] W. R. Fawcett, A. A. Kloss, Solvent-Induced Frequency Shifts in the Infrared Spectrum of Dimethyl Sulfoxide in Organic Solvents, The Journal of Physical Chemistry 100 (1996) 2019–2024.
- [89] K.-I. Oh, K. Rajesh, J. F. Stanton, C. R. Baiz, Quantifying Hydrogen-Bond Populations in Dimethyl Sulfoxide/Water Mixtures, Angew. Chem. Int. Ed. 56 (2017) 11375–11379.
- [90] M. Y. Skripkin, P. Lindqvist-Reis, A. Abbasi, J. Mink, I. Persson, M. Sandström, Vibrational spectroscopic force field studies of dimethyl sulfoxide and hexakis(dimethyl sulfoxide)scandium(III) iodide, and crystal and solution structure of the hexakis(dimethyl sulfoxide)scandium(III) ion, Dalton Trans. 0 (2004) 4038–4049.
- [91] N. S. Venkataramanan, A. Suvitha, Nature of bonding and cooperativity in linear DMSO clusters: A DFT, AIM and NCI analysis, Journal of Molecular Graphics and Modelling 81 (2018) 50–59.
- [92] M. L. Huggins, Thermodynamic Properties of Solutions of Long Chain Compounds, Annals of the New York Academy of Sciences 43 (1942) 1–32.
- [93] P. J. Flory, Thermodynamics of High Polymer Solutions, The Journal of Chemical Physics 10 (1942) 51–61.

- 993 [94] A. R. Miller, The Vapour-Pressure Equations of Solutions and the Os-  
994 motic Pressure of Rubber, Mathematical Proceedings of the Cambridge  
995 Philosophical Society 39 (1943) 54.
- 996 [95] K. Mizuno, S. Imafumi, T. Ochi, T. Ohta, S. Maeda, Hydration of  
997 the CH Groups in Dimethyl Sulfoxide Probed by NMR and IR, The  
998 Journal of Physical Chemistry B 104 (2000) 11001–11005.
- 999 [96] H.-C. Chang, J.-C. Jiang, C.-M. Feng, Y.-C. Yang, C.-C. Su, P.-J.  
1000 Chang, S. H. Lin, High-pressure spectroscopic probe of hydrophobic  
1001 hydration of the methyl groups in dimethyl sulfoxide, The Journal of  
1002 Chemical Physics 118 (2003) 1802–1807.
- 1003 [97] E. Mrázková, P. Hobza, Hydration of Sulfo and Methyl Groups in  
1004 Dimethyl Sulfoxide Is Accompanied by the Formation of Red-Shifted  
1005 Hydrogen Bonds and Improper Blue-Shifted Hydrogen Bonds: An ab  
1006 Initio Quantum Chemical Study, The Journal of Physical Chemistry  
1007 A 107 (2003) 1032–1039.
- 1008 [98] L. Qingzhong, N. Wang, Y. Zhiwu, Effect of hydration on the C-H...O  
1009 hydrogen bond: A theoretical study, Journal of Molecular Structure:  
1010 THEOCHEM 847 (2007) 68–74.
- 1011 [99] Q. Li, X. An, B. Gong, J. Cheng, Spectroscopic and theoretical evi-  
1012 dence for the cooperativity between red-shift hydrogen bond and blue-  
1013 shift hydrogen bond in DMSO aqueous solutions, Spectrochimica Acta  
1014 Part A: Molecular and Biomolecular Spectroscopy 69 (2008) 211–215.

- 1015 [100] Q. Li, X. An, B. Gong, J. Cheng, Comparison of contribution  
1016 of OH $\cdots$ OS hydrogen bond and CH $\cdots$ O<sub>w</sub> interaction to the methyl  
1017 blueshift in hydration of dimethyl sulfoxide, Vibrational Spectroscopy  
1018 46 (2008) 28–33.
- 1019 [101] J. Stangret, T. Gampe, Hydration of tetrahydrofuran derived from  
1020 FTIR spectroscopy, Journal of Molecular Structure 734 (2005) 183–  
1021 190.
- 1022 [102] A. Panuszko, E. Gojło, J. Zielkiewicz, M. Śmiechowski, J. Krakowiak,  
1023 J. Stangret, Hydration of Simple Amides. FTIR Spectra of HDO and  
1024 Theoretical Studies, The Journal of Physical Chemistry B 112 (2008)  
1025 2483–2493.
- 1026 [103] R. McMullan, G. A. Jeffrey, Hydrates of the Tetra *n*-butyl and Tetra  
1027 *i*-amyl Quaternary Ammonium Salts, The Journal of Chemical Physics  
1028 31 (1959) 1231–1234.
- 1029 [104] R. K. McMullan, M. Bonamico, G. A. Jeffrey, Polyhedral Clathrate  
1030 Hydrates. V. Structure of the Tetra-*n*-butyl Ammonium Fluoride Hy-  
1031 drate, The Journal of Chemical Physics 39 (1963) 3295–3310.
- 1032 [105] M. Bach-Vergés, S. J. Kitchin, K. D. M. Harris, M. Zugic, C. A. Koh,  
1033 Dynamic Properties of the Tetrahydrofuran Clathrate Hydrate, Inves-  
1034 tigated by Solid State <sup>2</sup>H NMR Spectroscopy, The Journal of Physical  
1035 Chemistry B 105 (2001) 2699–2706.
- 1036 [106] W.-Y. Wen, Aqueous solutions of symmetrical tetraalkylammonium

<sup>1037</sup>

salts, in: R. A. Horne (Ed.), Water and Aqueous Solutions, Wiley-

<sup>1038</sup>

Interscience, New York, 1972, pp. 613–661.

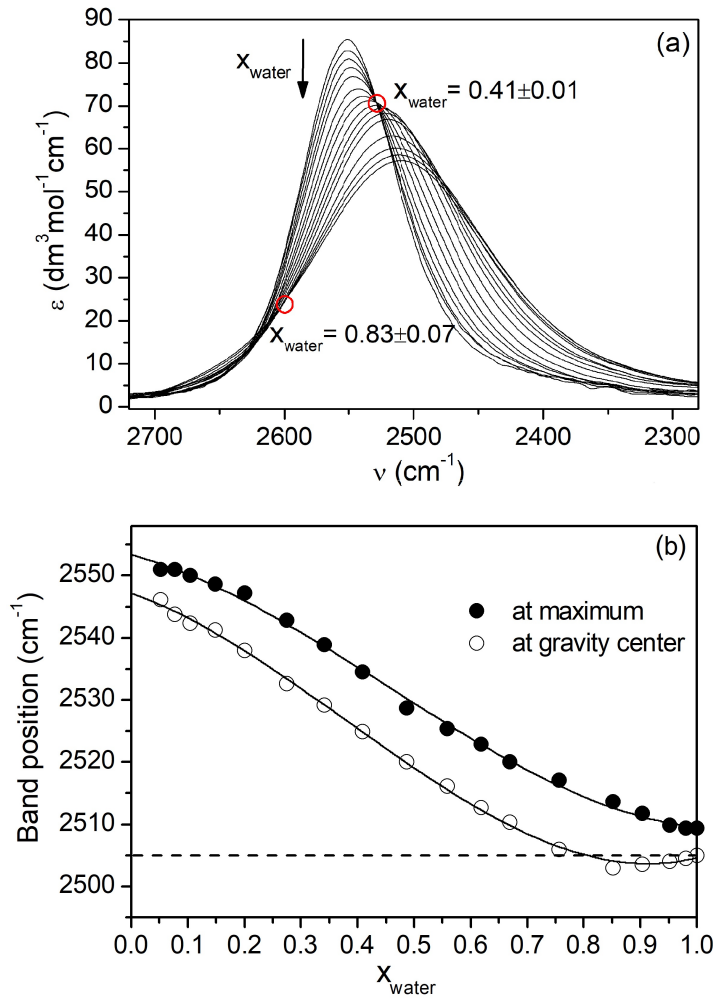


Figure 1: (a) Measured FTIR spectra of DMSO–water solutions at different mole fractions of water in the  $\nu(\text{OD})$  stretching vibrations range. The arrow shows increasing water mole fraction in the mixture. Red circles represent isosbestic points together with the corresponding water mole fractions:  $x_w = 0.41 \pm 0.01$  (the maximum mole fraction to which the spectra intersect) and  $x_w = 0.83 \pm 0.07$  (the minimum mole fraction from which the spectra begin to intersect). (b) The dependence of HDO band parameters on the mole fraction of water in the DMSO–water solutions. The dashed horizontal line denotes the band position at gravity center for pure water spectrum. Solid lines suggest the approximate relationship.

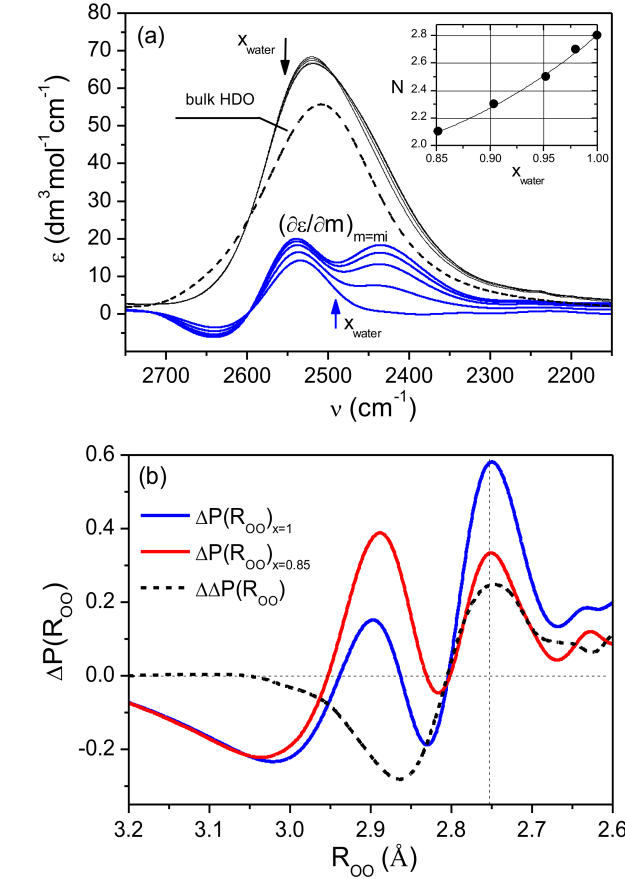


Figure 2: (a) DMSO-affected HDO spectra for high water content in mixtures, including the DMSO-affected HDO spectrum at the infinite dilution, for the water mole fractions as indicated in the inset (solid lines), along with the bulk HDO spectrum (black, dashed). Blue lines represent the derivatives  $(d\epsilon(\nu)/dm)_{m=m_i}$  for aqueous solutions of DMSO with molalities corresponding to the water mole fractions as indicated in the inset. The arrows indicate the direction of change of  $x_w$  in the mixture. Insert: The dependence of affected number,  $N$ , on the water mole fraction in the mixtures with the high water content. (b) Difference between interatomic oxygen-oxygen distance distribution function of DMSO-affected water at infinite dilution and the bulk water, (obtained on the basis of the spectra shown in Fig. 2a),  $\Delta P(R_{OO})_{x=1}$ , and the corresponding distance difference for the DMSO-affected water for high water content ( $x_w \simeq 0.85$ ) in the mixture (obtained on the basis of spectra in Fig. 2a),  $\Delta P(R_{OO})_{x=0.85}$ . The black dashed line shows the difference:  $\Delta\Delta P(R_{OO}) = \Delta P(R_{OO})_{x=1} - \Delta P(R_{OO})_{x=0.85}$ . The vertical dashed line corresponds to the oxygen-oxygen distance in ice-like water ( $2.76 \pm 0.01 \text{ \AA}$ ).

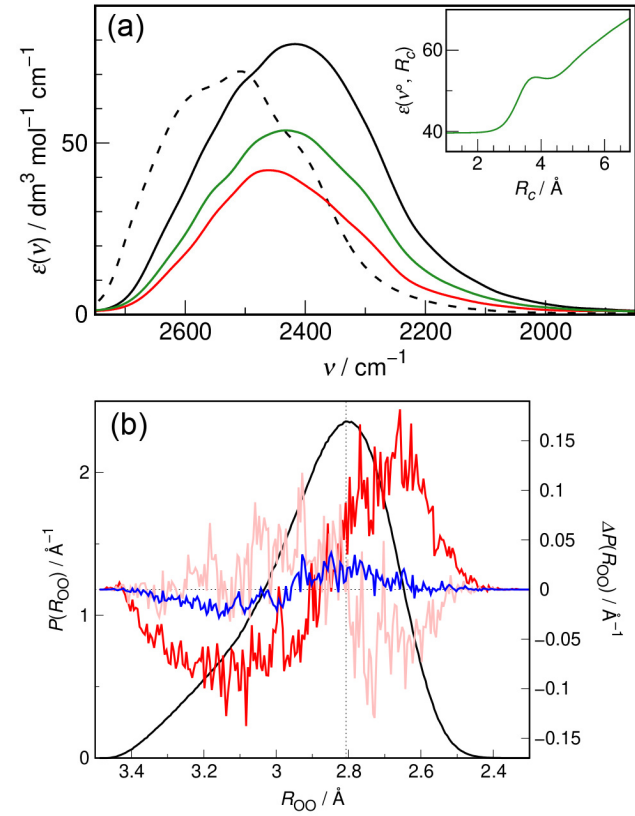


Figure 3: (a) Distance-dependent IR spectra from AIMD simulations at the cutoff radius  $R_c \rightarrow 0$  (i.e., DMSO molecule extracted from the solution, red) and  $R_c = 3.8 \text{ \AA}$  (green), together with the bulk  $\text{D}_2\text{O}$  spectrum (black) and the experimental IR spectrum of pure liquid  $\text{D}_2\text{O}$  (ref [80], black dashed). The inset shows the dependence of the intensity of the distance-dependent IR spectrum on  $R_c$  at the probing wavenumber  $\nu^\circ = 2461 \text{ cm}^{-1}$  (the position of the maximum at  $R_c \rightarrow 0$ ). (b) The interatomic oxygen–oxygen distance distribution function for hydrogen bonded water molecules in bulk  $\text{D}_2\text{O}$  (black, left ordinate axis),  $P(R_{OO})$ , together with the distance differences with respect to bulk  $\text{D}_2\text{O}$  (right ordinate axis),  $\Delta P(R_{OO})$ , for: water–water hydrogen bonds in the hydration shell of methyl groups of DMSO (up to  $4.7 \text{ \AA}$ , blue, cf. Fig. S10 and Table S2 in the Supplementary Material), water–water hydrogen bonds to water hydrogen bonded to the DMSO oxygen (up to  $3.5 \text{ \AA}$ , pink), as well as water–DMSO oxygen hydrogen bonds (red). See section S4.1 in the Supplementary Material for hydrogen bond definitions. The vertical dashed line corresponds to the oxygen–oxygen distance in bulk  $\text{D}_2\text{O}$  ( $R_{OO} \simeq 2.8 \text{ \AA}$ ).  
49

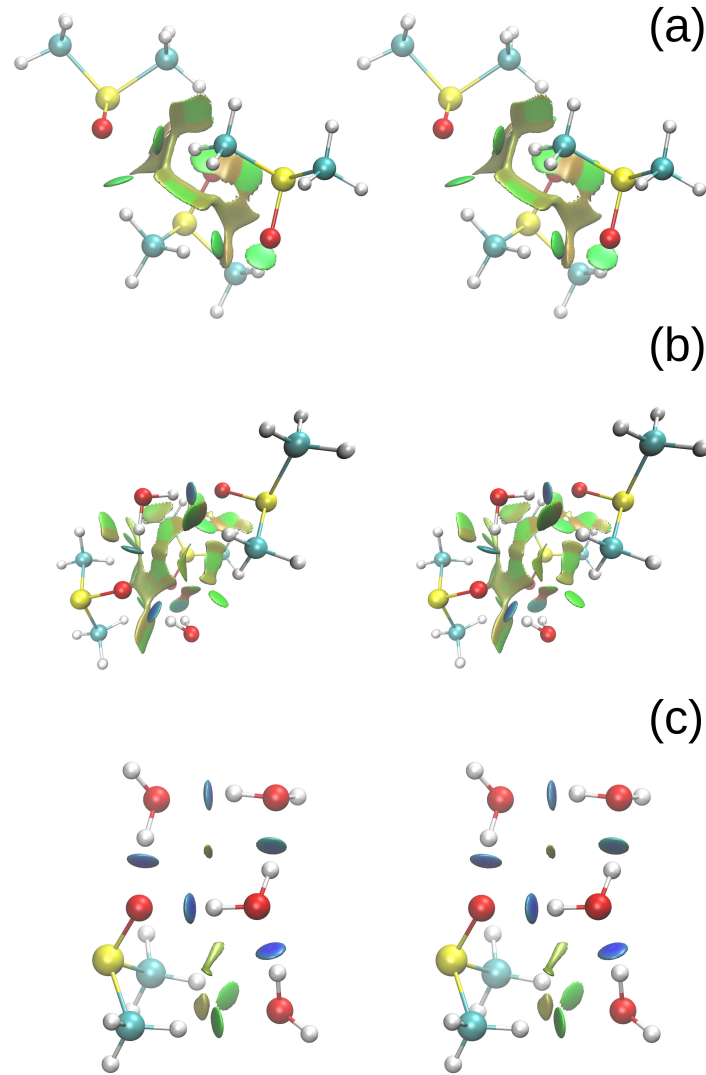


Figure 4: Stereo images of the results of weak interaction analysis of RDG function for (a) 3DMSO and small DMSO–water complexes: (b) 3DMSO·2H<sub>2</sub>O, chosen on the basis of the course of changes in the shape of SO band and results of WFA analysis, and (c) 1DMSO·4H<sub>2</sub>O, the first step of hydration sphere formation (the core type complex). Brown/olive flat, shapeless or elongated patches indicate van der Waals interactions, blue/green disks correspond to the hydrogen bonds (light green – weak HB, blue – strong HB). RDG calculated on the basis of electron densities obtained for DFT-optimized complexes in the CPCM model (B3LYP/6-311<sup>50</sup>+G(d,p)). See explanation in text.

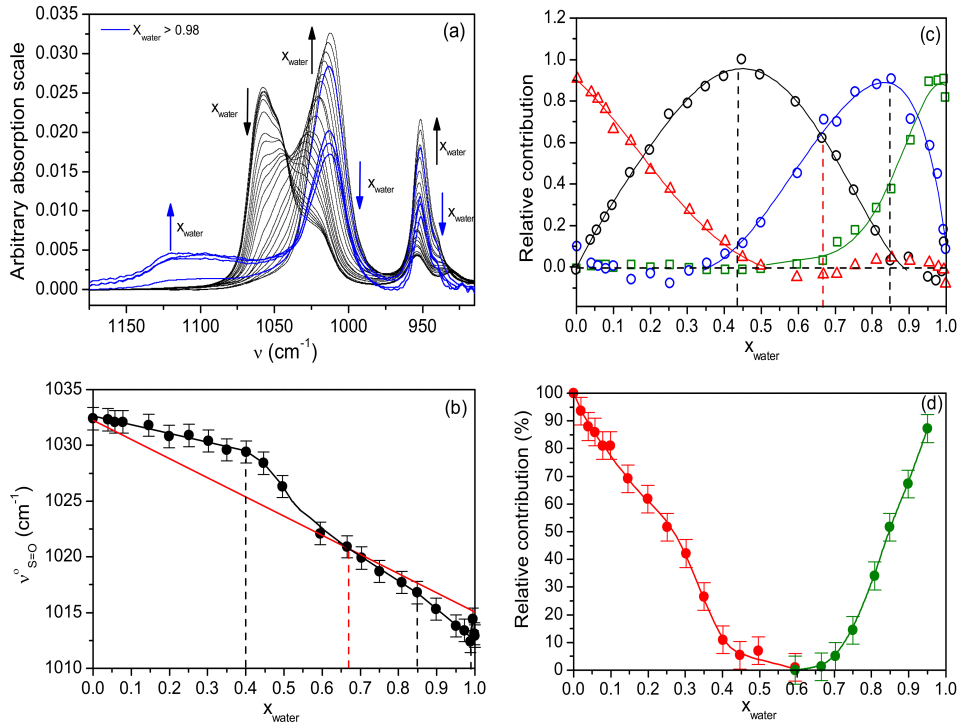


Figure 5: (a) FTIR spectra of DMSO–water mixtures in the range of the  $\nu(\text{S=O})$  and the rocking vibrations of the methyl groups depending on the solution composition. Blue lines represent the spectra for high water content in the mixtures ( $x_w > 0.98$ ). Increasing/decreasing water mole fraction is shown by arrows. (b) The dependence of the  $\nu(\text{S=O})$  band position in maximum for DMSO forming hydrogen bonds with water (based on the spectra shown in Fig. S1 in the Supplementary Material) on the mole fraction of water in DMSO–water solutions. In the set of these residual spectra for  $x_w > 0.1$ , both low-wavenumber component bands determine the maximum of the complex band of  $\nu(\text{S=O})$ . For  $x_w < 0.1$  the band position of the low-wavenumber component has been taken into account. Solid red line indicates hypothetical ideal solutions. Vertical dashed lines indicate the composition of complexes: red line denotes the eutectic composition [33], while the black lines correspond to the observed complexes at their maximum concentrations. (c) Relative contributions of different forms of DMSO as a function of water mole fraction from the factor analysis of DMSO–water spectra: DMSO non-bonded to water (red  $\triangle$ ); molecular complex 3DMSO·2H<sub>2</sub>O (black  $\circ$ ); molecular complex corresponding to the core type complex: 1DMSO·nH<sub>2</sub>O, where  $n = \frac{5}{6}$ , see text (blue  $\circ$ ); DMSO involved in the creation of the water cage (green  $\square$ ). (d) Relative contribution of DMSO not forming hydrogen bonds with water (red  $\bullet$ ), and DMSO involved in the creation of the water cage (green  $\bullet$ ) as a function of the mole fraction of water in DMSO–water solutions, obtained from the difference spectra method.

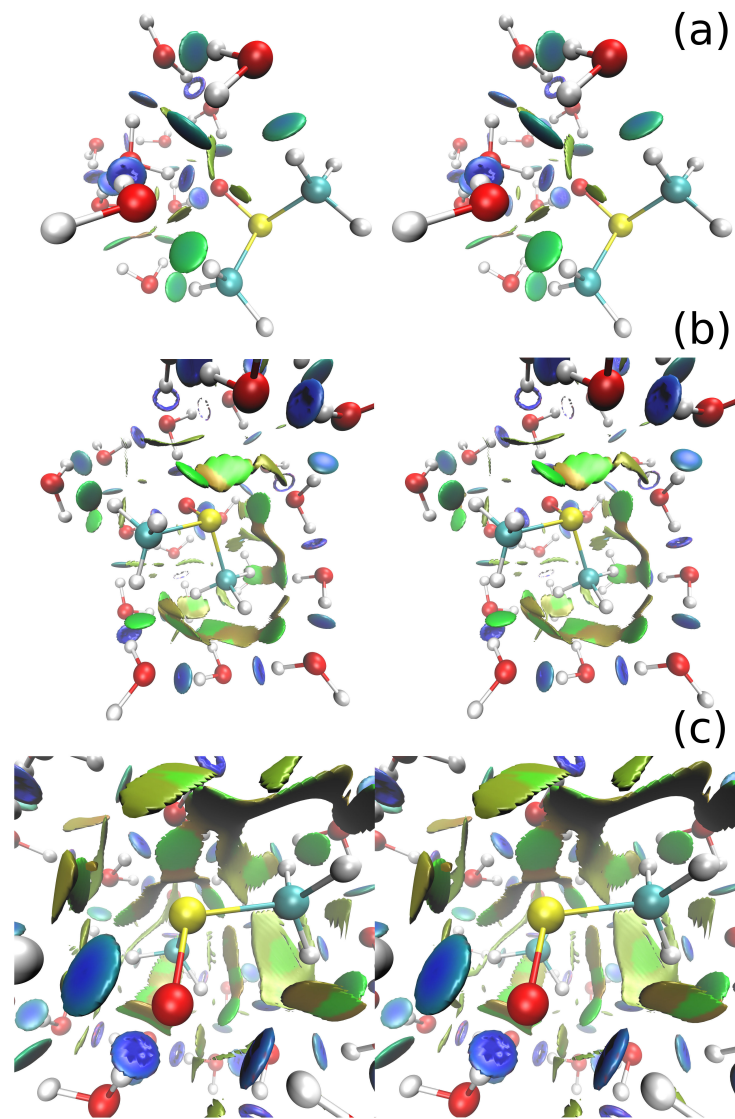


Figure 6: Stereo images of the results of weak interaction analysis by RDG function for larger DMSO–water complexes: a) 1DMSO·10H<sub>2</sub>O, b) 1DMSO·20H<sub>2</sub>O, c) 1DMSO·30H<sub>2</sub>O. The meaning of various structures and colours is the same as in Figure 4. RDG calculated on the basis of electron densities obtained for ONIOM-optimized (B3LYP/aug-cc-pVQZ and B3LYP/cc-pVDZ) systems for high and low level calculation, respectively. See explanation in text.

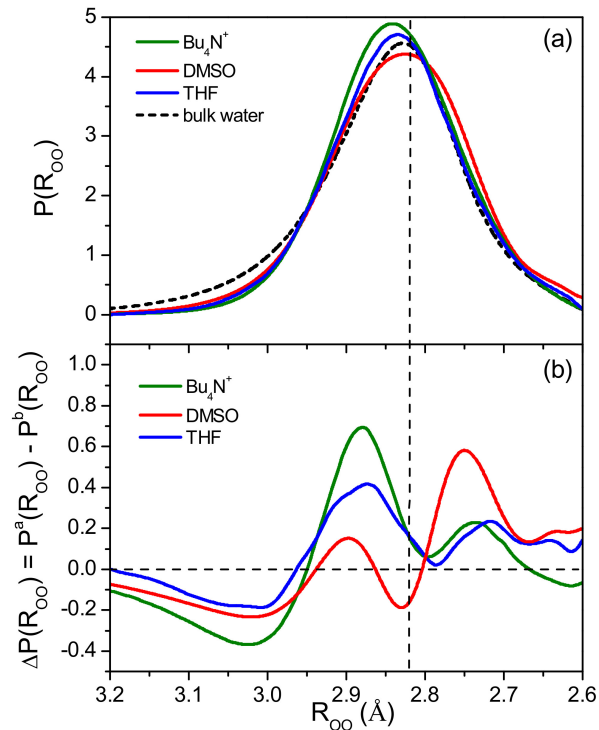


Figure 7: a) Interatomic oxygen–oxygen distance distribution function derived from the HDO spectra affected by DMSO,  $Bu_4N^+$  [44], and THF [101], together with the bulk HDO distance distribution curve. (b) Differences between interatomic oxygen–oxygen distance distribution function for solute-affected water,  $P^a(R_{OO})$ , and the bulk water,  $P^b(R_{OO})$ , for DMSO,  $Bu_4N^+$  [102], and THF. The vertical dashed line corresponds to the value of the most probable oxygen–oxygen distance in bulk water (2.83 Å).